mathematics

MDPI

Article

Real-World Data-Driven Machine-Learning-Based Optimal Sensor Selection Approach for Equipment Fault Detection in a Thermal Power Plant

Salman Khalid, Hyunho Hwang and Heung Soo Kim *

Department of Mechanical, Robotics and Energy Engineering, Dongguk University-Seoul, 30 Pil-dong 1 Gil, Jung-gu, Seoul 04620, Korea; salmankhalid@dongguk.edu (S.K.); gusgh1014@dongguk.edu (H.H.)
* Correspondence: heungsoo@dgu.edu; Tel.: +82-2-2260-8577; Fax: +82-2-2263-9379

Abstract: Due to growing electricity demand, developing an efficient fault-detection system in thermal power plants (TPPs) has become a demanding issue. The most probable reason for failure in TPPs is equipment (boiler and turbine) fault. Advance detection of equipment fault can help secure maintenance shutdowns and enhance the capacity utilization rates of the equipment. Recently, an intelligent fault diagnosis based on multivariate algorithms has been introduced in TPPs. In TPPs, a huge number of sensors are used for process maintenance. However, not all of these sensors are sensitive to fault detection. The previous studies just relied on the experts' provided data for equipment fault detection in TPPs. However, the performance of multivariate algorithms for fault detection is heavily dependent on the number of input sensors. The redundant and irrelevant sensors may reduce the performance of these algorithms, thus creating a need to determine the optimal sensor arrangement for efficient fault detection in TPPs. Therefore, this study proposes a novel machine-learning-based optimal sensor selection approach to analyze the boiler and turbine faults. Finally, real-world power plant equipment fault scenarios (boiler water wall tube leakage and turbine electric motor failure) are employed to verify the performance of the proposed model. The computational results indicate that the proposed approach enhanced the computational efficiency of machine-learning models by reducing the number of sensors up to 44% in the water wall tube leakage case scenario and 55% in the turbine motor fault case scenario. Further, the machine-learning performance is improved up to 97.6% and 92.6% in the water wall tube leakage and turbine motor fault case scenarios, respectively.

Keywords: real-world data; data-driven machine learning; thermal power plant; optimal sensor selection; boiler water wall tube; turbine; fault detection

Citation: Khalid, S.; Hwang, H.; Kim, H.S. Real-World Data-Driven Machine-Learning-Based Optimal Sensor Selection Approach for Equipment Fault Detection in a Thermal Power Plant. *Mathematics* **2021**, *9*, 2814. https://doi.org/10.3390/math9212814

Academic Editor: Victor Leiva

Received: 27 September 2021
Accepted: 4 November 2021
Published: 5 November 2021

1. Introduction

Modern thermal power plants are highly complex and are equipped with advanced data acquisition systems [1]. A huge amount of sensor data is generated and stored in the historical database of TPPs. These historical data represent the health state of the power plant that can be used for performance monitoring, fault detection, and isolation. The early detection and diagnosis of the faults in a thermal power plant can help implement shorter shutdowns, reduced maintenance, and lower generation costs [2].

Boiler tube leakage is the most probable failure in a thermal power plant. Approximately 60% of boiler shutdowns are caused by boiler tube leakages [3]. The most dominant occurrence of leakage occurs in the water wall tube section [4]. The tube leakage arises due to corrosion [5], erosion [5], and fatigue [6], which cause the tube wall thickness to decrease, leading to tube rupture and failure. Recently, an e-maintenance-based system [7] utilizing the process monitoring data was introduced for an intelligent fault diagnosis in TPPS. The process control data can provide sufficient information for effective tube

leakage detection [8]. Jungwon et al. [9] utilized the thermocouples sensors data mounted on the final superheater outlet header of an 870 MW coal-fired power plant and proposed a principal component analysis (PCA)-based tube leakage detection approach. The proposed method could successfully detect tube leakage. Recently, Natarianto et al. [10] used process control data and introduced a data analytics-based approach by combining PCA, canonical variate, and linear discriminant analysis (LDA) for water wall tube leakage detection in a 650 MW supercritical coal-fired thermal power plant. Swiercz et al. [11] proposed a multiway PCA approach for boiler riser and downcomer tube leakage detection using expert-provided sensor data. The proposed method could successfully detect the tube leak 3–5 days before boiler shutdown.

Steam turbines are another vital piece of equipment used as the primary energy-generating source in a thermal power plant [12]. Steam turbines consist of multistage steam expansion that makes them complex dynamic structures. The most common faults occurring in the steam turbine are unbalancing, gear fault, looseness, and bearing fault [13]. These faults can stop the smooth operation of the steam turbine and jeopardize reliable power generation. Various research in the past decade has investigated efficient fault detection in steam turbines using historical process data or expert knowledge about the system. The anomalies in the process data can be recognized for each type of failure. Different failures can be further classified using supervised learning. Karim et al. [14] proposed a fault detection and diagnosis approach in an industrial 440 MW steam turbine using four sensitive monitoring parameters. Under challenging noise measurements, twelve major faults were successfully classified using adaptive neuro-fuzzy inference (ANFIS) classifiers. Arian et al. [15] used process monitoring data generated from an Indonesian government steam power plant and proposed a data-driven approach for fault detection in a steam turbine using a neural-network-based classifier.

Generally, a huge amount of sensors are used in power plants for process maintenance [16]. However, not all of these sensors are sensitive to fault detection. The studies mentioned above only depend on expert experience in selecting sensitive sensors to detect boiler and turbine faults. However, redundant and irrelevant sensors may influence multivariate algorithms that are highly reliant on the number of input sensors. Thus, an accurate methodology is needed to select the relevant sensors necessary to detect boiler and turbine failures. Recently, machine-learning algorithms have gained importance for intelligent fault detection and diagnosis in thermal power plants [17]. These machine-learning algorithms are typically combined with dimensionality reduction methods, such as PCA, to eliminate unnecessary data [18,19]. However, these approaches do not help identify the cause of failure, nor do they distinguish the most relevant sensors. The feature selection approaches can overcome the challenges mentioned above by simultaneously identifying the relevant sensors and removing different feature selection techniques that are available in the literature, which can be categorized into three categories: optimization-based feature selection [20], regression-based feature selection [21], and classification-based feature selection [22]. For a TPP application, the optimal sensor selection algorithm should have lower complexity and computational cost. For that purpose, correlation analysis is a well-known approach that estimates the relationship between the pairwise input by using the correlation function and removing the redundant and irrelevant features [23]. Recently, the maximum relevance minimum redundancy (mRMR) algorithm [24] has gained importance, due to its simultaneous ability to minimize redundancy while controlling relevancy among the features. Extra tree classifier [25] is another feature selection technique that has gained popularity among researchers because of its explicit meaning, simple properties, and easy conversion to "if–then rules". This technique is helpful in problems involving a vast number of numerical features. Therefore, this study utilizes the above-mentioned three approaches for the optimal sensor arrangement in TPPs.

This paper proposes a data-driven machine-learning-based optimal sensor selection approach for thermal power plant boiler and turbine faults. The study performs optimal

sensor selection via different feature selection techniques (correlation, mRMR, and extra-tree classifier). Three supervised machine-learning classifiers (support vector machines, k-nearest neighbor, and naïve Bayes) are used for the fault classification. In the end, two real-world power plant equipment fault scenarios (boiler water wall tube leakage and turbine electric motor failure) are employed to verify the performance of the proposed model.

State-of-the-Art Literature Survey

This section lists the state of the art techniques used for equipment (boiler and turbine) fault detection in TPPs. Due to the significant importance of the boiler and turbine in TPPs, numerous attempts have been made to detect the equipment fault detection in TPP by using three main approaches, namely, the model-based method [26], the knowledge-based method [27], and the statistical analysis method [28]**.** A model-based approach is a conventional approach that uses static and dynamic models of the processes. In most cases, it can provide an efficient solution for fault detection. However, it cannot give correct fault detection results because it is difficult to obtain a correct mathematical model due to the complex operations of industrial systems. For a complex system with unknown models, a knowledge-based approach can be used to detect faults. This approach utilizes the rich industrial operational experience of the operators and includes the expert system method. However, this approach cannot identify the most sensitive process variables (sensors) needed to detect the faults in TPPs. Recently, statistical techniques based on multivariate algorithms such as PCA and ANNS are being used to monitor the processes with a large number of variables, such as in TPPs. However, the performance of these multivariate algorithms is highly dependent on the number of input process variables. Therefore, this study proposes an optimal sensor selection approach to identify the most sensitive sensors needed to detect equipment faults in TPPs. Table 1 covers the state of the art literature survey for the three main approaches (model-based, knowledge-based, and statistical analysis) used for boiler and turbine fault detection in TPP.

Table 1. State-of-the-art literature survey boiler and turbine fault detection in TPP.

Approach	Application	Year	Contribution	Limitation
Model-based approach	Boiler tube leakage detection [26]	1997	Developed the least-square method with forgetting factor derivation for leak detection	- Challenging to obtain a valid process mathematical model
	Boiler tube leakage detection [29]	2008	Developed the input/output loss method by computing fuel chemistry, heating value, and fuel flow	
	Turbine fault detection [30]	2012	Used the time-delay multilayer perceptron model for residual generation for fault detection in industrial turbine	
	Turbine fault detection [31]	2011	A nonlinear dynamic model with a dynamic tracking filter was used to detect turbine fault	
Knowledge-based approach	Boiler tube leakage detection [27]	1998	Used radiation heat flux measurements for boiler tube leak detection	- Experts provided sensors data - Unknown important monitoring process variables (sensors)
	Boiler tube leakage detection [32]	2016	Developed artificial neural network (ANN) models to detect tube leak	

	Turbine fault detection [13]	2017	Developed artificial neural network (ANN) models to detect a fault in steam turbine	
Statistical analysis approach	Boiler tube leakage detection [11]	2020	Used multiway PCA model to detect boiler tube leakage	- Performance highly dependent on the number of input sensor variables - Need to find optimal sensors necessary for fault detection
	Boiler tube leakage detection [9]	2017	Applied PCA to tube temperature data to detect boiler tube leakage	
	Turbine fault detection [15]	2011	A generalized discriminant analysis approach is used for steam turbine fault detection	
	Turbine fault detection [23]	2011	Proposed a support vector machine (SVM)-based model for fault detection in steam turbine	

2. Overview of a Coal-Fired Thermal Power Plant

The current study is conducted for a coal-fired TPP. This section gives a brief introduction of a TPP and covers the significance of the boiler and the steam turbine in a TPP.

The modern thermal power plants are developed to a great extent, but the essential equipment in a TPP is more or less the same, with a lot of sophistication and advancement to increase efficiencies [33]. Figure 1 shows the essential equipment in a coal-fired TPP. Steam is generated in the boiler and provided to the steam turbine. The steam turbine expands the steam and rotates the generator to supply electricity. The condenser condenses the turbine steam by transferring the heat to the cooling water supplied from the cooling tower.

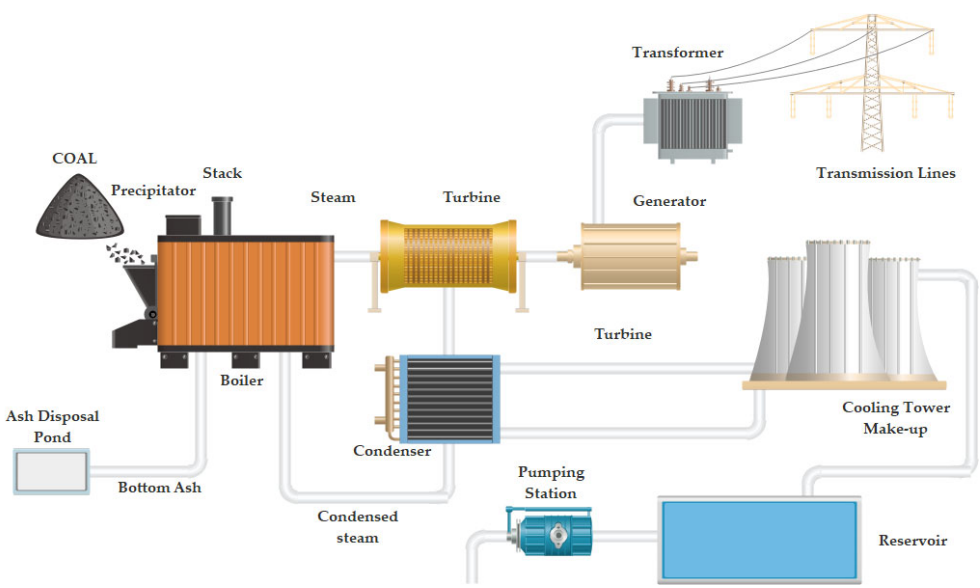

Figure 1. Essential equipment in a coal-fired TPP.

2.1. Boiler Water Wall Tube Leakage and its Significance in a Thermal Power Plant

Bursting of the boiler water wall tube is a severe threat to the continuous and smooth operation of a TPP. In a recent survey conducted by Kokkinos et al. [34], water wall tube leakage is the dominant failure mode in the different TPPs, followed by the final

superheater (SH III), first reheater (RH I), and the first superheater (SHI), as Figure 2 shows. Boiler tube leaks represent 52% of the total outages in a TPP.

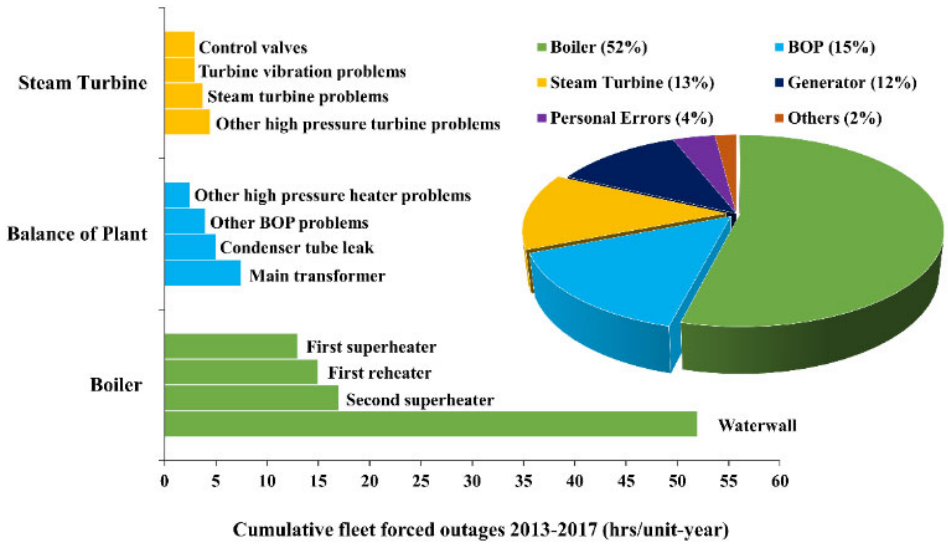

Figure 2. Survey of power plant faults representing the severity of the power plant faults and outage percentages.

A TPP shutdowns, whether planned or unplanned, can cause significant financial losses among which boiler tube leakage is the most dominant failure to cause power plant shutdowns. An extensive repairing cost ranging from 2 to 10 million dollars is typically required to repair these leaks [29]. Yong et al. [35] utilized the decision-tree-based method to carry out the cost analysis of the economizer tube leaks in TPP. Considering the electricity market price of 25 dollars/MWh, the expected repair prices are shown for different repair time intervals (repair immediately, delay two days, delay four days, and delay six days). By delaying the repair, the amount of expected repair cost increased significantly.

The water wall tubes are located close to the furnace, and due to the presence of high operating temperature, flue ash erosion, and creep, tube leakage occurs. Liu et al. [36] found that the water wall tube bursts because of overheating under high operating pressure. Yang et al. [37] investigated the coal quality and found that the coal used in TPPs has high ash content that causes corrosion in water wall tubes. It was concluded that suitable coal blending could reduce the corrosion in water wall tubes. Similarly, Xue [38] et al. analyzed the boiler water and found that the presence of NaOH causes corrosion-induced perforation leakage in water wall tubes. To prevent water wall tube leakage, power plant inspectors should inspect water quality to avoid tube leakage, and water quality testing should be performed regularly.

2.2. Turbine Motor Failure Analysis

The reliability of the steam turbine is highly dependent on the reliable functioning of its hydraulic lubrication and control oil system [39]. An essential requirement is a reliable oil supply over the whole operating range. The oil pumps used for that purpose provide the lube oil [40]. The oil pumps are directly driven by an electric motor (AC supply). In the absence of oil supply, bearing failure of the rotating machinery in the steam turbine can occur. This usually happens when an electric pump-driven motor fails due to a power failure or malfunction of the protection system. Therefore, the reliability of the main oil pump depends to a large extent on the AC electric motor. Different studies have been

carried out to analyze the AC electric motors [41]. It was found that 40 percent of the failures of AC motor occur due to the failure of the rolling bearing [42]. Therefore, it is recommended to diagnose the bearing condition on time, before failure occurs [43]. The other most prevalent faults in AC motors are winding, unbalanced stator and rotor, broken rotor bar, and eccentricity [44].

Recently, data-driven condition-based monitoring has gained importance in TPPs for efficient fault detection and diagnosis [45]. There are two main steps involved in condition-based monitoring. The first step consists of the data acquisition phase, which represents the health state of the object. For process control and monitoring, there are many sensors employed on the different components in the power plant. This sensor data can provide healthy and faulty state patterns that can be distinguished and classified using multivariate algorithms. In the second step, data preprocessing is carried out that involves multivariate algorithms to classify the preprocessed data. Thus, water wall tube leakage and turbine motor fault detection can be considered classification problems.

3. The Proposed Methodology

This section covers the proposed optimal sensor selection methodology and fault detection by using supervised machine-learning algorithms. The study is divided into three phases. In the first phase, the sensors that are essential for fault detection are distinguished by TPP experts. Those sensors are acquired and preprocessed for the optimal sensor selection process. The second phase utilizes the optimal sensor selection techniques to determine the most sensitive sensors. In the last phase, machine-learning algorithms are employed to detect the equipment (boiler and turbine) faults in TPPs and evaluate the performance of the sensor selection algorithms. The schematic of the proposed methodology is shown in Figure 3.

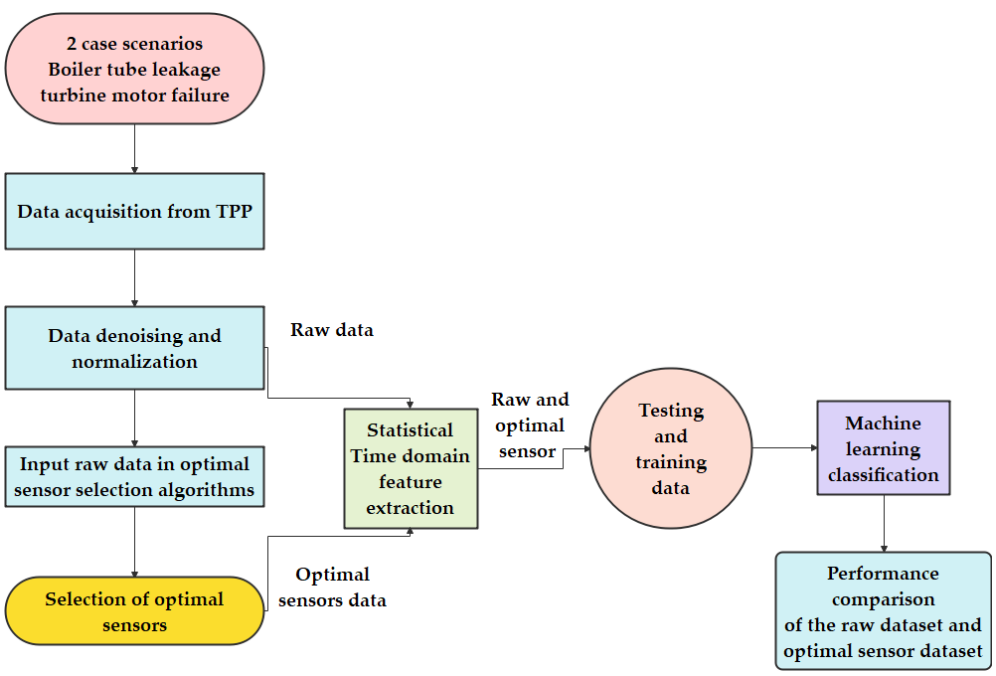

Figure 3. Schematic of the overall methodology.

3.1. Data Acquisition and Preprocessing

In a TPP, it is difficult to learn the exact moment of a fault occurrence, such as a tube leakage location, and the severity of the tube leakage. Therefore, the fault detection algorithm must estimate the appropriate sensors for fault detection. Power plant historical process control data consist of thousands of process variables (sensors). However, none

of those sensors are sensitive to specific faults. Therefore, the essential monitoring parameters should be carefully chosen for efficient fault detection. Power plant experts with years of experience usually carry out this process.

Power plant data tend to be inconsistent and noisy; therefore, data preprocessing is required [46]. In the literature, different noise removal techniques are being used. The traditional methods include Fourier transform analysis [47] and power spectral density analysis [48]. However, these techniques are more sensitive towards hidden oscillation and cannot obtain hidden frequencies. On the other hand, wavelet denoising has recently gained popularity in data denoising, because of its capability to simultaneously analyze both the time and frequency domains [49,50]. The wavelet works by decomposing the signal in the time and frequency domains. The selection of an optimal threshold is required to optimize the noise removal. Equation (1) shows the wavelet transform of the continuous signal:

$$\mathrm{WT.}(a,b) = \int_{-\infty}^{\infty} \mathrm{x(t)}\,\overline{\psi}\left(\frac{\mathrm{t}-b}{a}\right)\mathrm{dt} \tag{1}$$

where ψ(t) is the analyzing wavelet, a is the scale parameter, and b is the position parameter.

3.2. Optimal Sensor Selection

In a TPP, piping and instrumentation (P&ID) diagrams monitor all the sensors and equipment. Figure 4 shows the P&ID diagram of the low-pressure (LP) turbine section. There are six thermocouple sensors with unique sensor IDs attached on the furnace wall at separate locations. Similarly, in the P&ID diagram of the LP turbine, six thermocouple sensors are connected to the LP turbine casing. These localized attached sensors may contain redundant knowledge, thus influencing the performance of the multivariate algorithms. Therefore, it is important to downsize the input sensors and determine the appropriate sensor arrangement for equipment fault detection in a TPP.

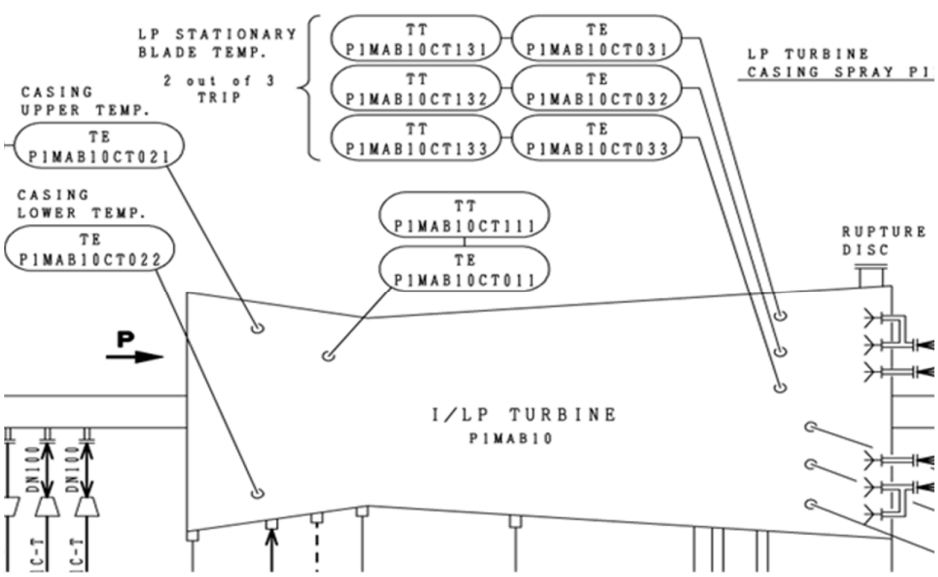

Figure 4. P&ID diagram of the LP turbine section in a TPP.

This study used three different optimal sensor selection approaches (correlation analysis, mRMR algorithm, and extra-tree classifier). The details of the approaches are as follows.

3.2.1. Correlation Analysis

Correlation analysis is a well-known technique and is usually preferred because of its ease of implementation, lesser complexity, and lower computational cost [51]. This analysis evaluates the strength and relationship between the two sensors [52]. Pearson's coefficient values range (−1 to 1). The value of 1 represents a high positive correlation, while −1 represents a negative correlation between the two sensors. Equation (2) shows how Pearson's correlation (r) coefficient is calculated:

$$r = \frac{s(\sum a\, b) - (a)(\sum b)}{\sqrt{\sqrt{\left[[s\sum b^2 - (\sum b)^2]\right][s\sum a^2 - (\sum a)^2]}}} \tag{2}$$

where s is the sensor data size, and a and b are the two input sensor variables.

The sensors with high correlation represent the same data trend, and removing the highly correlated sensor may not influence the functioning of the multivariate algorithms. Therefore, in this study, highly correlated sensors are discarded, while keeping one of the highly correlated sensors. The step-by-step implementation of the correlation analysis for the selection of optimal sensors is shown below:

1st step: Calculation of Pearson's correlation coefficient between all the sensor signals by using Equation (2).

2nd step: Construction of the correlation matrix representing the correlation between all the sensors.

3rd step: The sensors with a correlation value equal to or greater than 0.95 are considered highly correlated.

4th step: Highly correlated sensors are discarded while keeping one of the highly correlated sensors.

3.2.2. mRMR Algorithm

mRMR is an approach recently proposed by Peng et al. [53] and has gained considerable importance in mechanical fault diagnosis and structural health monitoring. mRMR selects the best features in the workspace by minimizing redundancy and maximizing relevancy. It exhibits fast calculation and strong robustness qualities [54]. Hence, our study adopted this method to find the optimal sensors needed for effective fault detection in a TPP. The theoretical background of the mRMR algorithm is summarized as follows.

The algorithm first calculates the mutual information between the attributes X and Y to quantify the relevance and redundancy. Mutual information is defined as follows:

$$I(X,Y) = \iint p(x,y)\, log \frac{p(x,y)}{p(x)p(y)} \tag{3}$$

where *p(x,y)* is the joint probabilistic density, and *p(x)* and *p(y)* are marginal probabilistic densities.

Let S denote the sensor dataset, while S_s represents the already selected sensor dataset that contains m sensors, and S_t denotes the to-be-selected sensors, with the dataset consisting of n sensors. The relevance D of the sensor f in S_t with the target c can be calculated as:

$$D = I(f, c) \tag{4}$$

The redundancy R of the sensor f in S_t with all the sensors in S_s can be calculated as:

$$R = \frac{1}{m} \sum_{fi \in S_s} I(f, c) \tag{5}$$

To obtain the sensor f_j in S_t with maximum relevancy and minimum redundancy, Equations (5) and (6) are combined with the mRMR function:

$$\max_{f_j \in S_s} \left[I(f_j, c) - \frac{1}{m} \sum_{f_i \in S_s} I(f_j, f_i) \right] (j = 1,2 \dots n) \tag{6}$$

For the sensor dataset with $N(= m + n)$ sensors, the sensor evaluation will continue N rounds. After these evaluations, the optimal sensor set O by mRMR is obtained:

$$O = \{f_1', f_2' \dots, f_h' \dots, f_n'\} \tag{7}$$

The sensor index h represents the importance of the sensor. The more important the sensor, the smaller its index h.

The overall steps involved in the computation of optimal sensor selection by using the mRMR algorithm is described below:

1st step: Mutual information is computed between the sensors by using Equation (3).

2nd step: The relevancy and redundancy of the sensor are computed by Equations (4) and (5).

3rd step: Equation (6) is used to obtain the sensor with maximum relevancy and minimum redundancy.

4th step: Score is computed for each sensor to be evaluated, and the sensors with a high score are chosen as optimal sensors

3.2.3. Extra-Tree Classifier (ETC)

The extra-tree classifier is an ensemble learning technique that accumulates the results of multiple decorrelated decision trees. Each decision tree selects the optimal feature by splitting the data based on the entropy value. The entropy of the feature estimates the quality of the split, as shown in Equation (8). The features belonging to the same class have zero entropy value. Thus, the extra-tree classifier works by recursively selecting node splits with the lowest entropy value:

$$Entropy\ (E) = -\sum_{i=1}^{c} p_i \log_2(p_i) \tag{8}$$

where c is the number of class labels, and p_i is the portion of the samples that belong to class i.

This study uses the extra-tree classifier because of its simple properties, easy conversion to "if–then" rules, and randomizing property for numerical input [25]. Such advantages make an extra-tree classifier useful for many input sensors and, in such situations, may increase accuracy. The step-by-step implementation of the extra-tree classifier is described as follows:

1st step: Computation of the entropy of the data by using Equation (8).

2nd step: Calculation of the total score for each sensor.

3rd step: Selection of the sensors with a high predictor importance score.

3.3. Machine-Learning Classifiers

Recently, supervised machine learning has gained importance in intelligent fault detection and condition monitoring [55]. Due to labeled data, the results generated from supervised machine learning are more accurate than that from other machine-learning types, such as unsupervised machine learning and reinforcement learning. In this study, three well-known supervised machine-learning classifiers (support-vector machine

(SVM), k-nearest neighbors (k-NN), and the naïve Bayes algorithm (NB)) are used for the fault classification.

Due to its tendency to avoid overfitting and its ability to solve complex problems, SVM is commonly used for fault detection applications [56]. SVM forms the hyperplane between the two classes and adjusts the boundary by expanding the distance between the two classes [57]. SVM uses the kernel functions [58] for the nonlinear and inseparable dataset cases. This study utilizes the RBF kernel function due to its higher robustness and infinite smoothness. k-NN is the second supervised machine-learning algorithm used in this study, which classifies the target by calculating its distance from the nearest feature space. k-NN is chosen in this study because of its ease of execution and requires no new parameters to tune. The third algorithm used in this study is naïve Bayes, which is based on the Bayesian theorem [59], and is commonly used for large datasets. Naïve Bayes is chosen in this study because of its higher classification speed and ease of implementation.

Before executing the machine-learning model in real-world applications, its performance must be estimated to verify its extrapolation ability and generalization. Different validation techniques are available in the literature, among which k-fold cross-validation is the most popular [60]. In this study, fivefold cross-validation is used to evaluate the training accuracies of the machine-learning models used.

4. Real-World Power Plant Scenarios—Computational Results

In this section, two real power plant fault case scenarios (boiler water wall tube leakage and turbine motor fault) are employed to validate the performance of the proposed approach. The fault case scenarios analyzed in this study are shown in Table 2.

Table 2. Description of fault case scenarios.

#	Fault Type	Fault Classification
1	TPP boiler water wall tube leakage	- Healthy state - Leakage state
2	TPP turbine motor failure	- Healthy state - Faulty state

The data obtained from the TPP consist of the time domain signals of the expert's selected process variables (sensors). The detailed description of the acquired data is shown in Figures A1 and A2. The process variables are stored in the historical database of a TPP with a sampling period of 1 s. Ten days of data at the normal working condition of the power plant and 10 days of data from the fault state were acquired from the TPP. As this study focused on the early-stage fault detection of TPP, the data should be provided according to the different fault severity levels so that the fault could be detected at the low severity level of the fault stage. However, the data were not acquired in controlled lab conditions. Therefore, it was not possible to create faults with different severity levels and obtain the data accordingly. This is the main limitation of the acquired data from TPP. Figure 5 shows a schematic of the proposed model for TPP boiler water wall tube leakage detection.

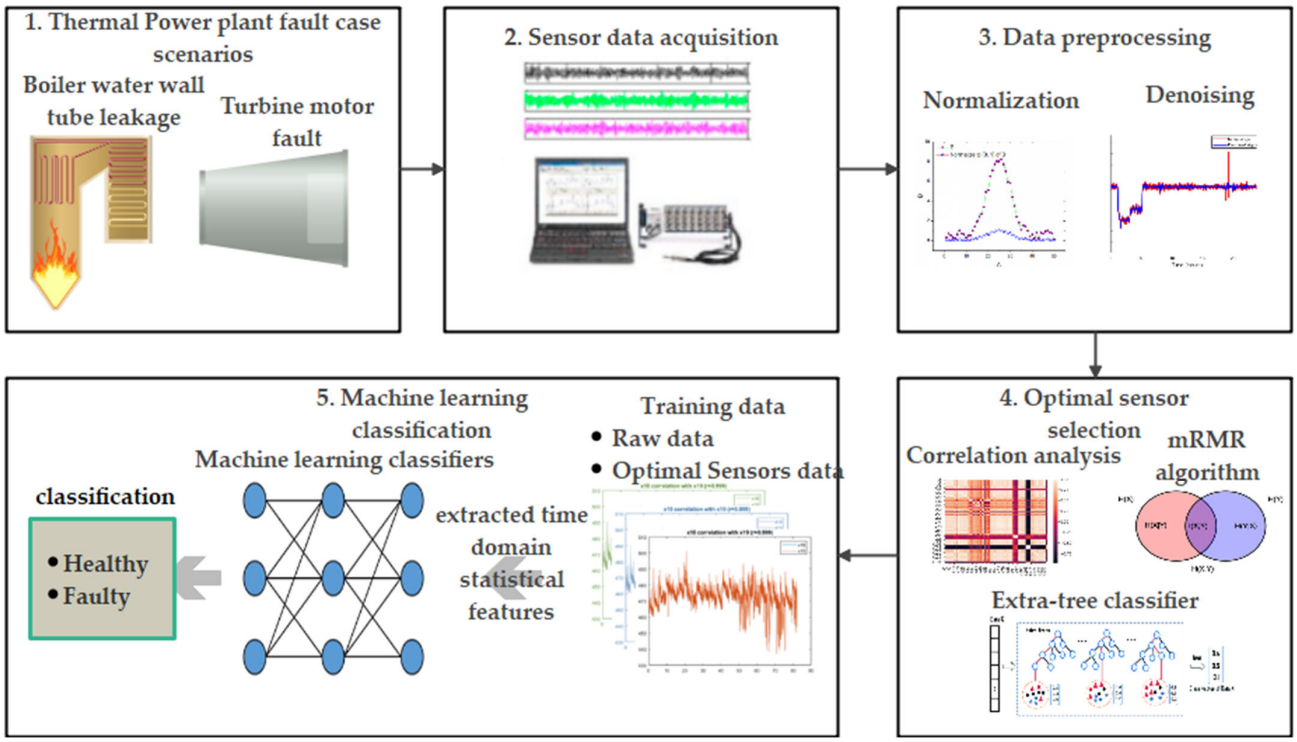

Figure 5. Detailed summary of the proposed approach.

4.1. Case Scenario 1—Boiler Water Wall Tube Leakage

This section implements the proposed approach to the real-world power plant boiler water wall tube leakage scenario. The details of the computational results are as follows.

4.1.1. Acquisition of the Sensitive Sensors Data and Data Preprocessing

Thirty-eight sensitive sensors selected by experts from 103 MW coal-fired thermal power plants are utilized in this study. The acquired sensors consist of a generator active power sensor and the thermocouple sensors employed in the different components of the boiler that measure inlet and outlet header temperatures, superheater (SHI, SHII, SHIII) metal temperatures, and reheater (RHI, RHII) metal temperatures. Figure A1 of Appendix A shows the details of the sensors with the power plant sensor ID, and the notations are assigned to each sensor for ease of the optimal sensor selection process.

Figure 6 shows the healthy (normal state) and leakage data plots for the SHI inlet header temperature, SHII metal temperature, and the RH II metal temperature with the corresponding generator active power. The data consist of the ten day (10 d) healthy and 10 d water wall tube leakage data acquired before the power plant shutdown. The red line represents the healthy data, whereas the blue color represents the leakage data. Large fluctuations are observed during the water wall tube leakage state of the boiler, as compared to the normal state.

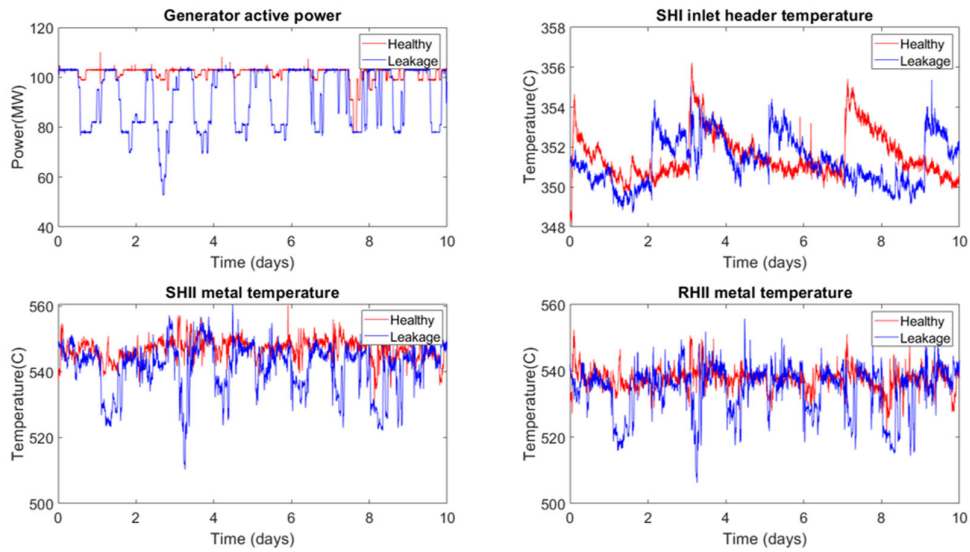

Figure 6. Thermocouple sensors data showing the healthy (normal) and the leakage state of the boiler with the corresponding generator active power.

After the data acquisition, data preprocessing was carried out. In the data preprocessing phase, the wavelet analyzer toolbox of MATLAB is used to denoise the sensor signals. Soft thresholding with five levels of decomposition was chosen for optimum noise removal. Figure 7 shows the effectiveness of the noise removal by wavelet denoising. The red color shows the denoised signal, while the black color line represents the noisy generator active power sensor signal.

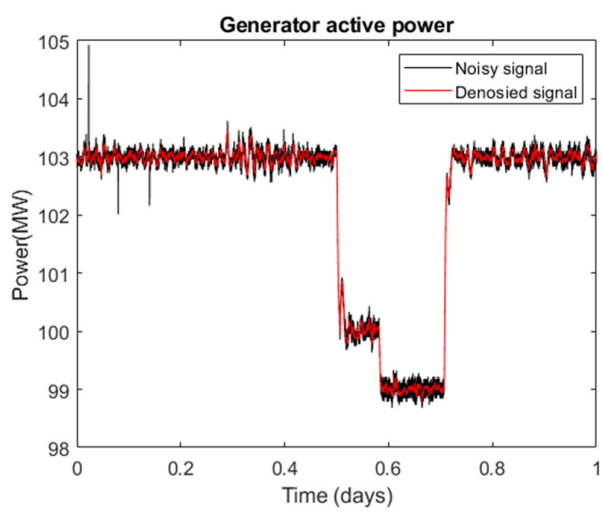

Figure 7. The noisy and denoised sensor signal showing the effectiveness of the wavelet denoising.

4.1.2. Optimal Sensor Selection Algorithms

Three different algorithms are used in this study for optimal sensor selection. The results of the algorithms are shown in each subsection.

1. Correlation analysis

The correlation analysis first carries out the optimal sensor selection process. Pearson's correlation coefficient is determined for all the data of the sensors. The sensors

showing a high correlation represent the same data trend, and the performance of the multivariate algorithm may not be influenced by keeping one of the highly correlated sensors and removing the rest. Two sensors are assumed to be highly correlated if the correlation coefficient value is > 0.95. Table 3 shows that X6 (steam temperature after SH I) is highly correlated with X7, X8, X9, X10, and X11 (SH I metal temperature) with the correlated coefficient value of >0.95. Therefore, X6 is selected, and the rest of the irrelevant sensors are removed. The exact process is carried out, and the 21 optimal sensors are selected out of 38 sensors.

Table 3. Sensors with high correlation coefficient values.

	Highly correlated sensors (SH II metal temperature)	Correlation coefficient value
X6 (Steam temperature after SH I)	X7	0.951
	X8	0.987
	X9	0.977
	X10	0.989
	X11	0.989
	X12	0.989

Figure 8 shows the correlation matrix with the 21 optimal sensors. The red color region shows the highly correlated sensors.

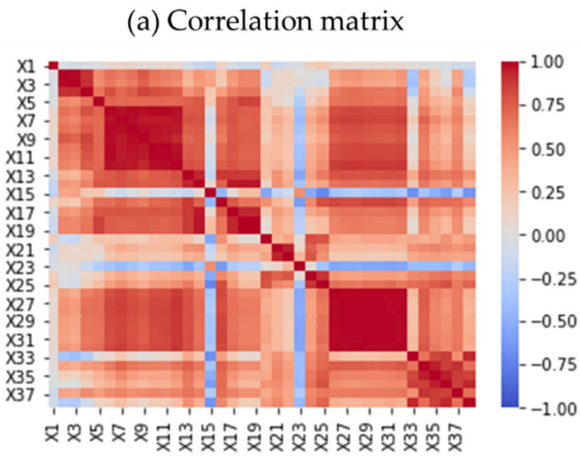

(b) Optimal sensors

Optimal sensor selected by correlation Analysis			
#	Tag ID	Tag description	Notation
1	P1CHA01GH001XQ01	Gen. active power	X1
2	P1HAH55CT002XQ01	SH I Inlet Header Temperature	X3
3	P1HAH55CT003XQ01	SH I Inlet Header Temperature	X4
4	P1HAH62CT001XQ01	Steam Temperature After SH I	X5
5	P1HAH62CT002XQ01	Steam Temperature After SH I	X6
6	P1HAH67CT001XQ01	SH II Metal Temperature	X13
7	P1HAH67CT002XQ01	SH II Metal Temperature	X14
8	P1HAH67CT003XQ01	SH II Metal Temperature	X15
9	P1HAH67CT004XQ01	SH II Metal Temperature	X16
10	P1HAH67CT005XQ01	SH II Metal Temperature	X17
11	P1HAH72CT003XQ01	Steam Temperature After SH II	X20
12	P1HAH77CT001XQ01	SH III Metal Temperature	X21
13	P1HAH77CT002XQ01	SH III Metal Temperature	X22
14	P1HAH77CT003XQ01	SH III Metal Temperature	X23
15	P1HAH77CT004XQ01	SH III Metal Temperature	X24
16	P1HAH77CT005XQ01	SH III Metal Temperature	X25
17	P1HAJ15CT001XQ01	RH I Metal Temperature	X26
18	P1HAJ35CT001XQ01	RH II Metal Temperature	X33
19	P1HAJ35CT002XQ01	RH II Metal Temperature	X34
20	P1HAJ35CT005XQ01	RH II Metal Temperature	X37
21	P1HAJ35CT006XQ01	RH II Metal Temperature	X38

Figure 8. (**a**) Correlation between the input sensors; (**b**) the optimal sensors selected after correlation analysis.

2. mRMR algorithm

The minimum redundancy and maximum relevance (mRMR) algorithm selects the optimal tags by selecting the relevant features, while controlling the redundancy within the selected features. Figure 9a represents the sensor rank with the predictor importance score. X25 with tag id P1HAH77CT005XQ01 representing the SH III metal temperature is on the 1st rank with the predictor importance score of 0.22, followed by X1 (generator active power). Figure 9b shows the 21 optimal sensors that are selected.

(a) mRMR algorithm optimal sensors

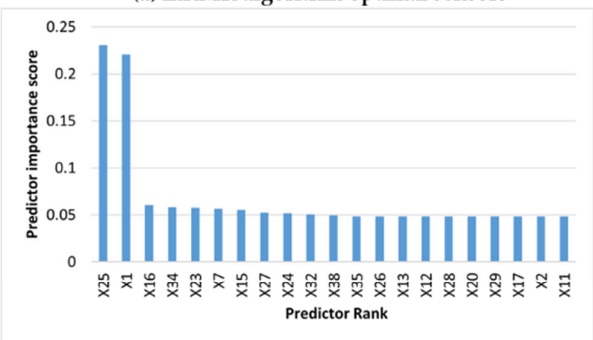

(b) Optimal sensors

Optimal sensor selected by mRMR Algorithm			
#	Tag ID	Tag description	Notation
1	P1HAH77CT005XQ01	SH III Metal Temperature	X25
2	P1CHA01GH001XQ01	Gen. active power	X1
3	P1HAH67CT004XQ01	SH II Metal Temperature	X16
4	P1HAJ35CT002XQ01	RH II Metal Temperature	X34
5	P1HAH77CT003XQ01	SH III Metal Temperature	X23
6	P1HAH57CT001XQ01	SH I Metal Temperature	X7
7	P1HAH67CT003XQ01	SH II Metal Temperature	X15
8	P1HAJ15CT002XQ01	RH I Metal Temperature	X27
9	P1HAH77CT004XQ0	SH III Metal Temperature	X24
10	P1HAJ20CT001XQ01	RH I Outlet Steam Tem-perature	X32
11	P1HAJ35CT006XQ01	RH II Metal Temperature	X38
12	P1HAJ35CT003XQ01	RH II Metal Temperature	X35
13	P1HAJ15CT001XQ01	RH I Metal Temperature	X26
14	P1HAH67CT001XQ01	SH II Metal Temperature	X13
15	P1HAH57CT006XQ01	SH I Metal Temperature	X12
16	P1HAJ15C003XQ01	RH I Metal Temperature	X28
17	P1HAH72CT003XQ01	Steam Tem-perature Af-ter SH II	X20
18	P1HAJ15C004XQ01	RH I Metal Temperature	X29
19	P1HAH57CT001XQ01	SH I Metal Temperature	X'7
20	P1HAH57CT006XQ01	SH I Metal Temperature	X12
21	P1HAH57CT005XQ01	SH I Metal Temperature	X11

Figure 9. (**a**) mRMR algorithm selected sensors; (**b**) optimal sensors selected by mRMR algorithm.

3. Extra-tree classifier

The extra-tree algorithm is a type of ensemble learning technique that aggregates multiple decorrelated decision trees to select the optimal tags. Figure 10a shows that the top 21 tags with high predictor importance are selected as optimal tags. X1 with tag id representing the active generator power is on the 1st rank with the predictor importance score of 0.185, followed by X25 (SH III metal temperature). Figure 10b shows the optimal sensors selected by the extra-tree classifier.

(a) Extra tree algorithm optimal sensors

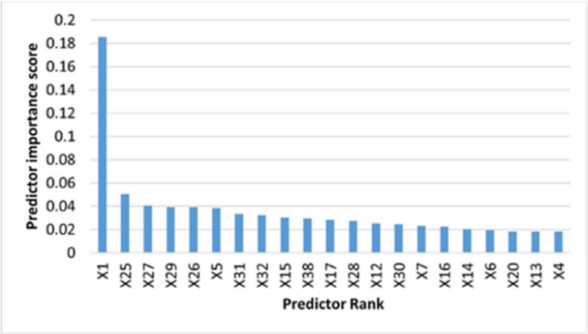

(b) Optimal sensors

Optimal sensors selected by Extra-tree classifier			
#	Tag ID	Tag description	Notation
1	P1CHA01GH001XQ01	Gen. active power	X1
2	P1HAH77CT005XQ01	SH III Metal Temperature	X25
3	P1HAJ15CT002XQ01	RH I Metal Temperature	X27
4	P1HAJ15CT004XQ01	RH I Metal Temperature	X29
5	P1HAJ15CT001XQ01	RH I Metal Temperature	X26
6	P1HAH62CT001XQ01	Steam Temperature After SH I	X5
7	P1HAJ15CT006XQ01	RH I Metal Temperature	X31
8	P1HAJ20CT001XQ01	RH I Outlet Steam Temperature	X32
9	P1HAH67CT003XQ01	SH II Metal Temperature	X15
10	P1HAJ35CT006XQ01	RH II Metal Temperature	X38
11	P1HAH67CT005XQ01	SH II Metal Temperature	X17
12	P1HAJ15C003XQ01	RH I Metal Temperature	X28
13	P1HAH57CT006XQ01	SH I Metal Temperature	X12
14	P1HAJ15CT005XQ01	RH I Metal Temperature	X30
15	P1HAH57CT001XQ01	SH I Metal Temperature	X7
16	P1HAH67CT004XQ01	SH II Metal Temperature	X16
17	P1HAH67CT002XQ01	SH II Metal Temperature	X14
18	P1HAH62CT002XQ01	Steam Temperature After SH I	X6
19	P1HAH72CT003XQ01	Steam Temperature After SH II (Aft Spary Valve)	X20
20	P1HAH67CT001XQ01	SH II Metal Temperature	X13
21	P1HAH55CT003XQ01	SH I Inlet Header Temperature	X4

Figure 10. (**a**) Extra-tree classifier selected sensors; (**b**) optimal sensors selected by the extra-tree classifier.

4.1.3. Machine-Learning Classification

This section presents the machine-learning performance of the proposed methodology. The sensor data (raw data) obtained from the power plant consists of 38 time-domain signals with 10 days of healthy and 10 days of leakage data. Twenty-one sensor signals (optimal sensors) are selected by each optimal sensor selection scheme (correlation analysis, mRMR algorithm, and extra-tree classifier). The direct application of the time-domain signals in the machine-learning classifiers cannot provide satisfactory results. Therefore, the common practice is to estimate the time-domain statistical features and use these features in the machine-learning classifiers. In this study, four time-domain statistical features (root mean square, variance, skewness, and kurtosis) are computed for the raw and optimal sensors data. Table 4 shows that four data cases are analyzed, and the machine-learning performance is computed and compared.

Table 4. Case scenarios for the machine-learning classification.

Case-1	Raw data	38 sensors
Case-2	Correlation analysis	21 sensors
Case-3	mRMR algorithm	21 sensors
Case-4	Extra-tree classifier	21 sensors

Fivefold cross-validation is performed to avoid overfitting. The data are partitioned into five disjointed folds. The fourfold data were used as the training samples, and the onefold data as a testing sample for each of the five iterations. This methodology provides a reasonable estimation of the predictive accuracy of the final model trained with all the data. Figure 11 summarizes the results of the machine-learning classification for all four case scenarios. Without implementing the optimal sensor selection, the k-NN-based classifier provides the highest machine-learning accuracy of 94.7%. It can be observed that after eliminating the irrelevant sensors, the performance of the machine-learning classifiers increased slightly in the optimal sensor data case scenarios. The k-NN-based mRMR algorithm provides the highest machine-learning accuracy of 97.6%.

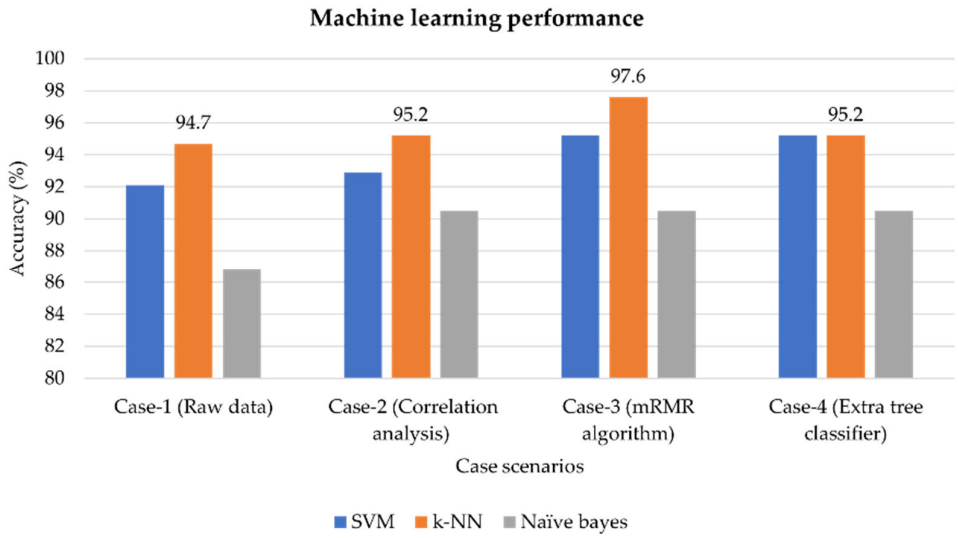

Figure 11. Machine-learning performance comparison of the four data case scenarios.

Figure 12 plots the confusion matrix for the k-NN-based raw data case scenario and the k-NN-based mRMR algorithm to assess the performance of the classifier in the raw and optimal sensor data case scenarios. The confusion matrix indicates the performance

of the classifier in each class. The row shows the true class, while the column shows the predicted class. The accuracy in the confusion matrix is calculated as follows:

$$\textbf{Accuracy} = \frac{\textbf{TP}}{\textbf{TP} + \textbf{FN}} \tag{9}$$

where **TP** represents the true positive, and **FN** represents the false negative.

In the raw data, 7.9% and 2.6% misclassification occur in the healthy (H) and water wall leakage (WWL) classes. In the optimal sensors data case scenario, the misclassification in each class is reduced to 4.8% in the healthy class, and k-NN classifies correctly for the water wall tube leakage class, with no misclassification error.

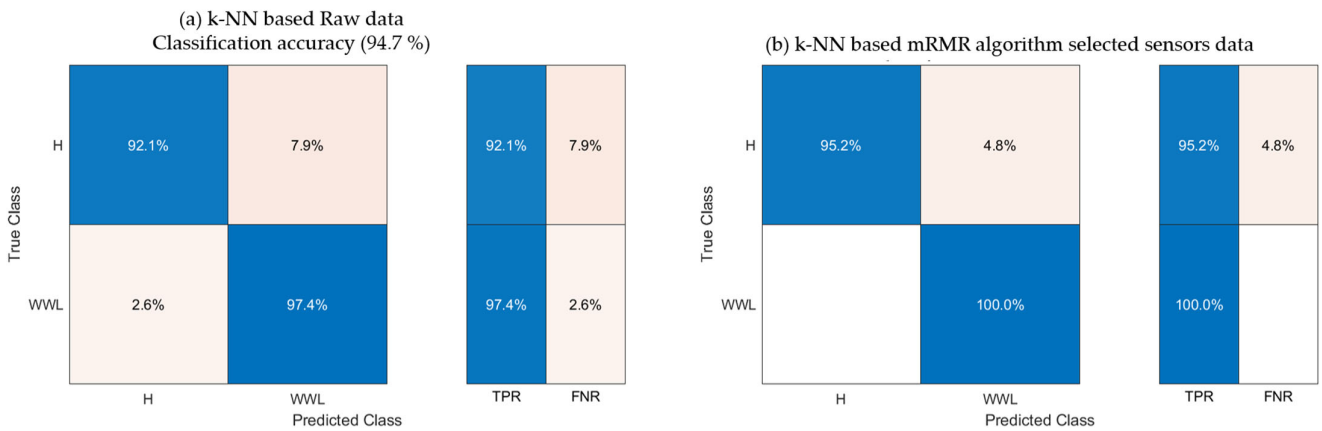

Figure 12. (**a**) Confusion matrix for the k-NN-based raw data case scenario; (**b**) confusion matrix for the k-NN-based mRMR algorithm case scenario.

In addition to fivefold cross-validation, tenfold cross-validation is performed to validate the robustness of the machine-learning models, and the results are compared with fivefold cross-validation results, as shown in Table 5. It was observed that there is a slight enhancement of cross-validation accuracies in tenfold cross-validation for both the raw and optimal sensor datasets.

Table 5. Comparison of fivefold and tenfold cross-validation accuracies for the boiler water wall tube leakage detection scenario.

	Fivefold Cross-Validation Accuracies (%)			**Tenfold Cross-Validation Accuracies (%)**		
	SVM	**k-NN**	**Naïve Bayes**	**SVM**	**k-NN**	**Naïve Bayes**
Raw data	92.1	94.7	86.8	93.4	94.7	88.1
Correlation analysis	92.9	95.2	90.5	94.3	95.7	91.2
mRMR algorithm	95.2	97.6	90.8	95.9	97.8	91.6
Extra-tree classifier	95.2	95.2	90.8	95.9	95.7	91.6

4.2. Case Scenario—2: Steam Turbine Motor Failure

In the second case scenario, this study analyzes the steam turbine motor failure for the 500 MW thermal power plant that resulted in the unscheduled maintenance shutdown. The proposed data-driven machine-learning-based optimal sensor selection approach is employed intelligently to diagnose the steam turbine motor fault detection.

4.2.1. Acquisition of the Sensitive Sensors Data and Data Preprocessing

Experts of the power plant provided the one hundred and 36 sensor data that are most sensitive to the steam turbine motor fault. Figure A2 of Appendix A shows the details of the sensor data. ID represents the number given to each sensor in the power plant. Notations are assigned to each sensor for the optimal sensor selection process.

The data consist of the 10 d healthy and the 10 d faulty state data, as shown in Figure 13. The different sensors (main turbine speed, vibration-X bearing#1, and HP exhaust steam temperature) are plotted corresponding to the active generator power. The red color represents the healthy data, whereas the blue color shows the faulty state of the turbine. It can be observed that during the faulty state of the steam turbine, the fluctuations in the sensor data increased.

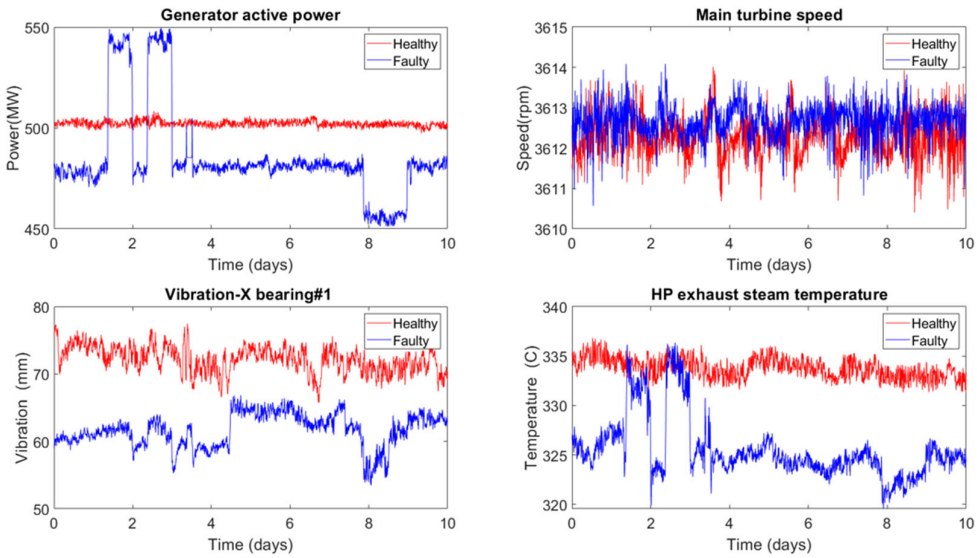

Figure 13. Sensor data showing the healthy (normal) and the faulty state of the steam turbine with the corresponding generator active power.

Similarly, as in the case-1 scenario, the wavelet analyzer toolbox is utilized to denoise the sensor signals. Figure 14 shows the effectiveness of the wavelet denoising. Black color represents the noisy signal, while the red color shows the denoised signal after employing the wavelet denoising.

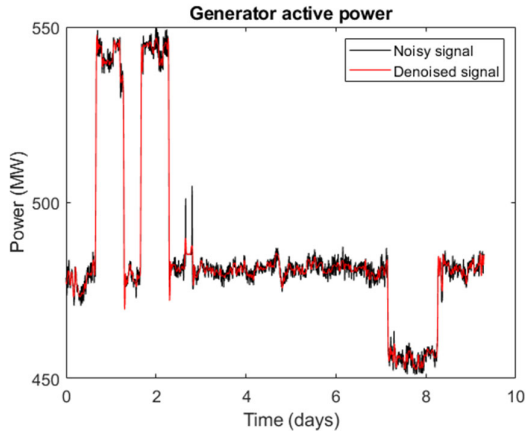

Figure 14. Wavelet denoising of the noisy data.

4.2.2. Optimal Sensor Selection

This section shows the computational results of the correlation analysis, mRMR algorithm, and the extra-tree classifier.

1. Correlation analysis

Pearson's correlation coefficient is computed for all the sensor signals. The high-correlation sensors are removed, while keeping one. The procedure is followed throughout the sensor selection process, and 61 optimal sensors are selected. Figure 15 shows the correlation matrix. The red color represents a high correlation between the sensors.

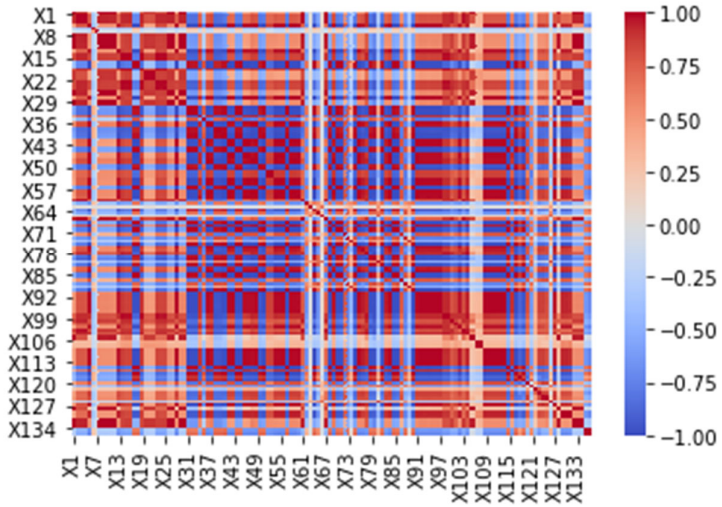

Figure 15. Correlation matrix of the sensitive sensor data.

Figure 16 shows the optimal sensors selected by correlation analysis consist of the actual load (generator active power), HP exhaust steam temperature, main turbine speed, bearing vibrations, bearing metal temperatures, and oil drain temperatures.

#	ID	Description	Notation	#	ID	Description	Notation
1	7DH-MW.XQ21	MW ACTUAL LOAD	X1	31	S7.ROTOR_EXP1	Rotor Expansion #1	X56
2	7DH-SPDO.XQ21	SPEED MAIN TBN	X6	32	7S1SED1.XQ31	SHELL EXPNSN	X57
3	S7.TT_ES	HP Exhaust Steam Temperature	X13	33	S7.DIFF1_EXP	Differential Expansion #1	X58
4	S7.TT_ES3	HP Exhaust Steam Temperature #3	X16	34	7S1ECCENT.XQ31	ECCENTRICITY	X60
5	S7.TT_HPEXHLI1	HP Exhaust Lower Inner Metal Temperature #1	X17	35	7CC-TT05.XQ01	T MAIN TBN LO CLR OUTL	X62
6	S7.TT_HPEXHLI2	HP Exhaust Lower Inner Metal Temperature #2	X18	36	7LO-TT32.XQ01	T MAIN TBN L/O FM CLR	X63
7	7CR-TT01A.XQ01	T CRH LN-A STM	X20	37	7S7-L71QAT	Lube Oil Tank Level Transmitter	X64
8	BFPT7A.A_AXIAL1	Axial Position #1	X31	38	7S1TT-G1M1.XQ31	TBN/GEN BRG #1 MTL TMP	X68
9	7S1BB1X.XQ31	VIB 1X - BRG #1	X34	39	7S1TT-G2M1.XQ31	TBN/GEN BRG #2 MTL TMP	X69
10	7S1BB1Y.XQ31	VIB 1Y - BRG #1	X35	40	7S1TT-G7M1.XQ31	TBN/GEN BRG #7 MTL TMP	X74
11	7S1BB2X.XQ31	VIB 2X - BRG #2	X36	41	7S1TT-G9M1.XQ31	TBN/GEN BRG #9 MTL TMP	X76
12	7S1BB2Y.XQ31	VIB 2Y - BRG #2	X37	42	7S1TT-TAM1.XQ31	TBN Thrust Active Upper MTL Temp	X77
13	7S1BB3X.XQ31	VIB 3X - BRG #3	X38	43	S7.TT_G1M1	Turbine/Generator Bearing #1 Metal Temperature #1	X83
14	7S1BB3Y.XQ31	VIB 3Y - BRG #3	X39	44	S7.TT_G2M1	Turbine/Generator Bearing #2 Metal Temperature #1	X84
15	7S1BB4X.XQ31	VIB 4X - BRG #4	X40	45	S7.TT_G9M1	Turbine/Generator Bearing #9 Metal Temperature #1	X91
16	7S1BB4Y.XQ31	VIB 4Y - BRG #4	X41	46	S7.TT_LPA1	Exhaust Hood A Gen end temperature #1	X92
17	7S1BB5X.XQ31	VIB 5X - BRG #5	X42	47	S7.TT_LPB1	Exhaust Hood B Gen end temperature #1	X95
18	7S1BB5Y.XQ31	VIB 5Y - BRG #5	X43	48	S7.TT_SSH	Steam Seal Header Temperature	X99
19	7S1BB6X.XQ31	VIB 7X - BRG #6	X44	49	S7.T2_HP	HP Turbine Rotor Bore Temperature	X100
20	7S1BB6Y.XQ31	VIB 6Y - BRG #6	X45	50	7HE-FT02A.XQ01	F IP EXT TO BFPT-A STM	X103
21	7S1BB7X.XQ31	VIB 7X - BRG #7	X46	51	7HE-FT02B.XQ01	F IP EXT TO BFPT-B STM	X104
22	7S1BB7Y.XQ31	VIB 7Y - BRG #7	X47	52	7HE-PT03A.XQ01	P IP EXT TO BFPT-A STM	X105
23	7S1BB8X.XQ31	VIB 8X - BRG #8	X48	53	7HE-TT01.XQ01	T IP EXT TO DEA STM	X108
24	7S1BB8Y.XQ31	VIB 8Y - BRG #8	X49	54	S7.EV_PA1	Exhaust Vacuum #1 LPA Hood	X109
25	7S1BB9X.XQ31	VIB 9X - BRG #9	X50	55	S7.HYD	Hydraulic Fluid Pressure	X115
26	7S1BB9Y.XQ31	VIB 9Y - BRG #9	X51	56	S7.HYD_PUR1	H2 Analyzer #1 Purity	X116
27	7S1BHDR.XQ31	BRG HDR PRES	X52	57	7S7-L71EQAT	HFP TANK OIL LEVEL Tx	X117
28	S7.BHDR	Bearing Header Pressure	X53	58	S7.SQP	Seal Oil Differential Pressure	X118
29	7S1DIFF1-EXP.XQ31	DIFF EXPNSN #1	X54	59	S7.TT_G1D	Bearing #1 Oil Drain Temperature	X119
30	7S1ROTOR-EXP1.XQ31	ROTR EXPNSN #1	X55	60	S7.TT_G9D	Bearing #9 Oil Drain Temperature	X127
				61	7HR-PT06A.XQ01	P DWNSTR LP BP RIGHT	X135

Figure 16. List of the optimal sensors selected by correlation analysis.

2. mRMR algorithm

The mRMR algorithm is applied to the sensor data to minimize the redundancy while keeping the relevance. Figure 17 shows the sensor rank with the predictor importance score. X25 with tag id P1HAH77CT005XQ01 representing the SH III metal temperature is on the 1st rank with a predictor importance score of 0.22, followed by X1 (generator active power). Figure 9b shows the 21 optimal sensors that are selected.

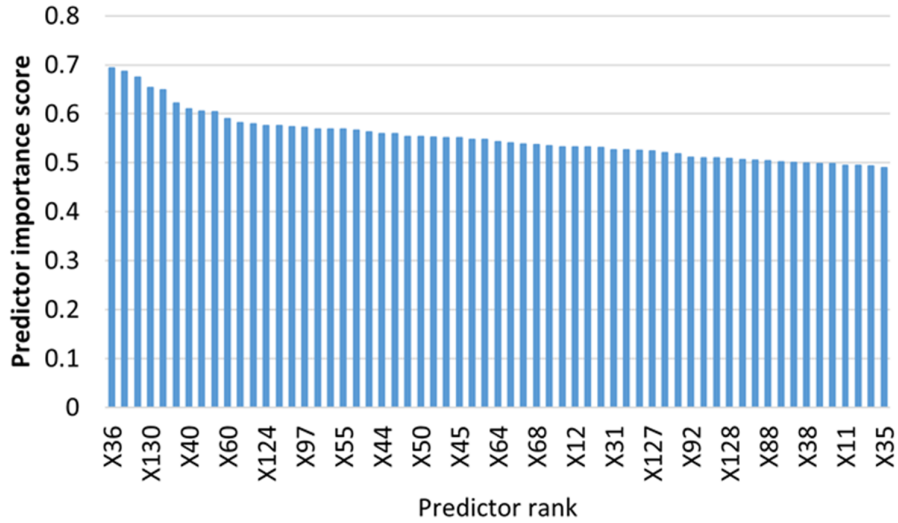

Figure 17. Optimal sensors ranking with the predictor importance score.

X36 (vibration-2X in bearing #2) is selected to be the most sensitive sensor with a predictor importance score of 0.698, followed by turbine bearing metal temperature #1. Figure 18 lists the 61 optimal sensors selected by the mRMR algorithm.

Rank	ID	Description	Notation	Rank	ID	Description	Notation
1	7S1BB2X.XQ31	VIB 2X - BRG #2	X36	31	7S7-L71QAT	Lube Oil Tank Level Transmitter	X64
2	S7.TT_G8M1	Turbine/Generator Bearing #8 Metal Temperature #1	X90	32	'S1TT-XOU-CS.XQ3:	C_OVER MTL TMP	X129
3	S7.TT_G9M1	Turbine/Generator Bearing #9 Metal Temperature #1	X91	33	7S1TT-TIM2.XQ31	TBN Thrust Inactive LWL MTL Temp	X80
4	7S1TT-XOU1.XQ31	CROSS OVER PIPE TEMP1	X130	34	7S1TT-G1M1.XQ31	TBN/GEN BRG #1 MTL TMP	X68
5	S7.TT_TID	Inactive Thrust Bearing Oil Drain Temperature	X82	35	7S1BB2Y.XQ31	VIB 2Y - BRG #2	X37
6	S7.ROTOR_EXP1	Rotor Expansion #1	X56	36	S7.TT_G7D	Bearing #7 Oil Drain Temperature	X125
7	7S1BB4X.XQ31	VIB 4X - BRG #4	X40	37	S7.TP_HPE_P	HP Exhaust Pressure	X12
8	7S1BB9Y.XQ31	VIB 9Y - BRG #9	X51	38	7S1TT-G8M1.XQ31	TBN/GEN BRG #8 MTL TMP	X75
9	S7.TT_G4M1	Turbine/Generator Bearing #4 Metal Temperature #1	X86	39	7S1BB1X.XQ31	VIB 1X - BRG #1	X34
10	7S1ECCENT.XQ31	ECCENTRICITY	X60	40	BFPT7A.A_AXIAL1	Axial Position #1	X31
11	7S1BB8X.XQ31	VIB 8X - BRG #8	X48	41	7S1TT-G4M1.XQ31	TBN/GEN BRG #4 MTL TMP	X71
12	S7.T2_XO	Reheat Exhaust Rotor Bore Temperature	X102	42	7S1BB4Y.XQ31	VIB 4Y - BRG #4	X41
13	S7.TT_G6D	Bearing #6 Oil Drain Temperature	X124	43	S7.TT_G9D	Bearing #9 Oil Drain Temperature	X127
14	7S1TT-TIM1.XQ31	TBN Thrust Inactive UPP MTL Temp	X79	44	S7.TT_LPA3	Exhaust Hood A Gen end temperature #3	X94
15	S7.BHDR	Bearing Header Pressure	X53	45	S7.TT_LPA3	Exhaust Hood A Gen end temperature #3	X94
16	S7.TT_LPB3	Exhaust Hood B Gen end temperature #3	X97	46	S7.TT_LPA1	Exhaust Hood A Gen end temperature #1	X92
17	7S1TT-XOU2.XQ31	CROSS OVER PIPE TEMP2	X131	47	7S1BB7Y.XQ31	VIB 7Y - BRG #7	X47
18	S7.TT_LOCIA	LUBE OIL COOLER INLET TEMP	X65	48	S7.TT_SSH	Steam Seal Header Temperature	X99
19	7S1ROTOR-EXP1.XQ31	ROTR EXPNSN #1	X55	49	7S1XOP.XQ31	Cross Over Pipe Press	X128
20	7S1TT-TAM1.XQ31	TBN Thrust Active Upper MTL Temp	X77	50	S7.TT_LPB1	Exhaust Hood B Gen end temperature #1	X95
21	7DH-MW.XQ21	MW ACTUAL LOAD	X1	51	BFPT7A.A_AXIAL3	Axial Position #3	X33
22	7S1BB6X.XQ31	VIB 7X - BRG #6	X44	52	S7.TT_G6M1	Turbine/Generator Bearing #6 Metal Temperature #1	X88
23	7HE-FT02B.XQ01	F IP EXT TO BFPT-B STM	X104	53	7S1FSP.XQ31	1STG SHELL PRES	X61
24	S7.TT_G5M1	Turbine/Generator Bearing #5 Metal Temperature #1	X87	54	7S7-L71EQAT	HFP TANK OIL LEVEL Tx	X117
25	7S1BB9X.XQ31	VIB 9X - BRG #9	X50	55	7S1BB3X.XQ31	VIB 3X - BRG #3	X38
26	S7.TT_HPEXHLI1	HP Exhaust Lower Inner Metal Temperature #1	X17	56	7S1TT-G3M1.XQ31	TBN/GEN BRG #3 MTL TMP	X70
27	S7.TT_G5D	Bearing #5 Oil Drain Temperature	X123	57	7S1BB5X.XQ31	VIB 5X - BRG #5	X42
28	7S1BB6Y.XQ31	VIB 6Y - BRG #6	X45	58	7CR-PT03B.XQ01	P HP TBN EXH-2	X11
29	7S1TT-TAM2.XQ31	TBN Thrust Active Lower MTL Temp	X78	59	7S1BB8Y.XQ31	VIB 8Y - BRG #8	X49
30	S7.TT_LPA2	Exhaust Hood A Gen end temperature #2	X93	60	7CC-TT05.XQ01	T MAIN TBN LO CLR OUTL	X62
				61	7S1BB1Y.XQ31	VIB 1Y - BRG #1	X35

Figure 18. List of optimal sensors selected by mRMR algorithm.

3. Extra-tree classifier

The raw sensors (136 sensors) are given as the input in the extra-tree classifier. The top 61 are selected as the optimal sensors necessary to predict turbine motor fault. Figure 19 presents the predictor importance score of the selected sensors. X37 (bearing#2 vibration-2Y) is selected as the most sensitive sensor variable with a predictor importance score of 0.062.

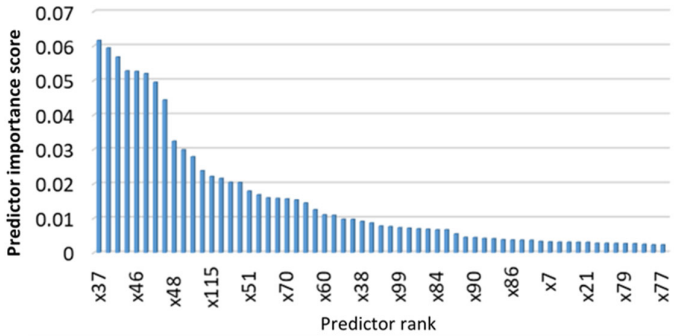

Figure 19. Optimal sensor ranking with the predictor importance score.

Figure 20 lists the complete sensors selected by the extra-tree classifier according to the predictor rank.

Rank	ID	Description	Notation	Rank	ID	Description	Notation
1	7S1BB2Y.XQ31	VIB 2Y - BRG #2	X37	31	S7.TT_SSH	Steam Seal Header Temperature	X99
2	7S1BB2X.XQ31	VIB 2X - BRG #2	X36	32	7CR-PT03A.XQ01	P HP TBN EXH-1	X10
3	7S1BB3Y.XQ31	VIB 3Y - BRG #3	X39	33	S7.TT_HPEXHLI1	HP Exhaust Lower Inner Metal Temperature #1	X17
4	7S1BB7X.XQ31	VIB 7X - BRG #7	X46	34	S7.TT_G2M1	Turbine/Generator Bearing #2 Metal Temperature #1	X84
5	S7.TT_G9D	Bearing #9 Oil Drain Temperature	X127	35	S7.DIFF1B_EXP	Differential Expansion #1B	X59
6	7S1BB5Y.XQ31	VIB 5Y - BRG #5	X43	36	S7.EV_PB1	Exhaust Vacuum #1 LPB Hood	X112
7	7CR-TT01A.XQ01	T CRH LN-A STM	X20	37	S7.TT_G8M1	Turbine/Generator Bearing #8 Metal Temperature #1	X90
8	7S1TT-XOU2.XQ31	CROSS OVER PIPE TEMP2	X131	38	S7.ROTOR_EXP1	Rotor Expansion #1	X56
9	BFPT7A.A_AXIAL1	Axial Position #1	X31	39	7S1SED1.XQ31	SHELL EXPNSN	X57
10	7S1BB1X.XQ31	VIB 1X - BRG #1	X34	40	S7.DIFF1_EXP	Differential Expansion #1	X58
11	7S1BB1Y.XQ31	VIB 1Y - BRG #1	X35	41	S7.TT_G4M1	Turbine/Generator Bearing #4 Metal Temperature #1	X86
12	S7.HYD	Hydraulic Fluid Pressure	X115	42	7CR-TT03B.XQ01	T CRH LN-B STM	X25
13	7HE-TT02A.XQ01	T IP EXT TO BFPT-A STM	X107	43	7S1TT-G1M1.XQ31	TBN/GEN BRG #1 MTL TMP	X68
14	7S1BB4X.XQ31	VIB 4X - BRG #4	X40	44	7S1TT-G2M1.XQ31	TBN/GEN BRG #2 MTL TMP	X69
15	7S1BB4Y.XQ31	VIB 4Y - BRG #4	X41	45	S7.TT_G9M1	Turbine/Generator Bearing #9 Metal Temperature #1	X91
16	7S1BB5X.XQ31	VIB 5X - BRG #5	X42	46	7S1TNH-RPM.XQ31	HP TBN SPD (RPM)	X7
17	7S1BB9Y.XQ31	VIB 9Y - BRG #9	X51	47	7HR-PT05B.XQ01	P UPSTR LP BP_B	X133
18	7S1BB6X.XQ31	VIB 7X - BRG #6	X44	48	7S1TT-G4M1.XQ31	TBN/GEN BRG #4 MTL TMP	X71
19	7S1BB6Y.XQ31	VIB 6Y - BRG #6	X45	49	7S1TT-G7M1.XQ31	TBN/GEN BRG #7 MTL TMP	X74
20	7S1BB7Y.XQ31	VIB 7Y - BRG #7	X47	50	7S1TT-G9M1.XQ31	TBN/GEN BRG #9 MTL TMP	X76
21	7S1BB8X.XQ31	VIB 8X - BRG #8	X48	51	7CR-TT02A.XQ01	T CRH LN-A STM	X21
22	7S1TT-G3M1.XQ31	TBN/GEN BRG #3 MTL TMP	X70	52	S7.TT_LPA3	Exhaust Hood A Gen end temperature #3	X94
23	7S1BB8Y.XQ31	VIB 8Y - BRG #8	X49	53	S7.HYD_PUR1	H2 Analyzer #1 Purity	X116
24	7S1BB9X.XQ31	VIB 9X - BRG #9	X50	54	7S7-L71EQAT	HFP TANK OIL LEVEL Tx	X117
25	7S1ROTOR-EXP1.XQ31	ROTR EXPNSN #1	X55	55	S7.SQP	Seal Oil Differential Pressure	X118
26	7S1ECCENT.XQ31	ECCENTRICITY	X60	56	S7.TT_TAD	Active Thrust Bearing Oil Drain Temperature	X81
27	7S1BHDR.XQ31	BRG HDR PRES	X52	57	7S1TT-TIM1.XQ31	TBN Thrust Inactive UPP MTL Temp	X79
28	S7.BHDR	Bearing Header Pressure	X53	58	S7.TT_G1M1	Turbine/Generator Bearing #1 Metal Temperature #1	X83
29	7S1BB3X.XQ31	VIB 3X - BRG #3	X38	59	S7.TT_LPB3	Exhaust Hood B Gen end temperature #3	X97
30	7S1DIFF1-EXP.XQ31	DIFF EXPNSN #1	X54	60	S7.TT_G3M1	Turbine/Generator Bearing #3 Metal Temperature #1	X85
				61	7S1TT-TAM1.XQ31	TBN Thrust Active Upper MTL Temp	X77

Figure 20. List of optimal sensors selected by extra-tree algorithm.

4.2.3. Machine-Learning Classification

This section computes machine-learning performance to quantify the proposed machine-learning-based optimal sensor selection approach. The raw data obtained from the power plant consists of 136 sensors with 10 d of data for each healthy and faulty state. The data consist of the time-domain signals; therefore, the four statistical features (root mean square, variance, skewness, and kurtosis) are calculated for the raw and optimal sensors data and used in the machine-learning classifiers to attain satisfactory results. Table 6 shows that four data cases are analyzed, and the machine-learning performance is computed and compared.

Table 6. Case scenarios for the machine-learning classification.

Case-1	Raw data	136 sensors
Case-2	Correlation analysis	61 sensors
Case-3	mRMR algorithm	61 sensors
Case-4	Extra-tree classifier	61 sensors

Three supervised machine-learning classifiers (SVM, k-NN, and naïve Bayes) are chosen in this study to classify the normal and leakage state. Fivefold cross-validation is performed to avoid overfitting. Figure 21 summarizes the results of the machine-learning classification for all four case scenarios. Without implementing the optimal sensor selection, the naïve-Bayes-based machine-learning classifier provides the highest machine-learning accuracy of 87.5%. After removing the irrelevant sensors, the performance of the machine-learning classifiers increased slightly in the optimal sensor data case scenarios. The naïve-Bayes-based extra-tree classifier provides the highest machine-learning accuracy of 92.6%. The machine-learning performance of the naïve Bayes classifier increased to 5.1%, compared to the raw sensor dataset case. Therefore, the proposed machine-learning-based optimal sensor selection approach enhanced the classification performance and reduced the input sensors to 55.1%.

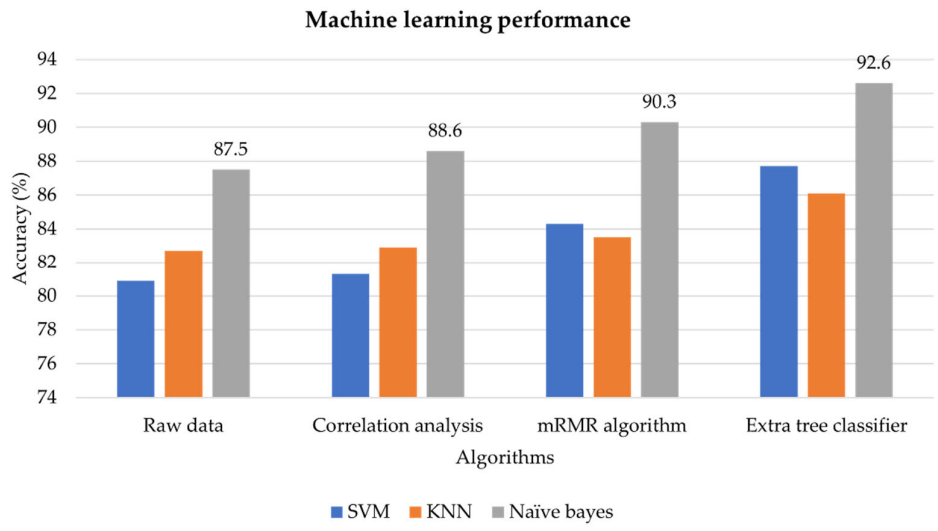

Figure 21. Machine-learning performance comparison of the four data case scenarios.

Figure 22 shows the confusion matrix for the naïve-Bayes-based raw data case scenario and plots the extra-tree classifier to assess the classifier performance in the raw and optimal sensor data case scenarios. This indicates that in the raw data case scenario, the false-negative rate is 19.1% in the fault class (f) and 5.9% in the healthy class (h). The naïve Bayes algorithm reduced the false-negative rate to 6% and 4.3% in healthy and fault classes, respectively, and enhanced the machine-learning performance to 92.6%.

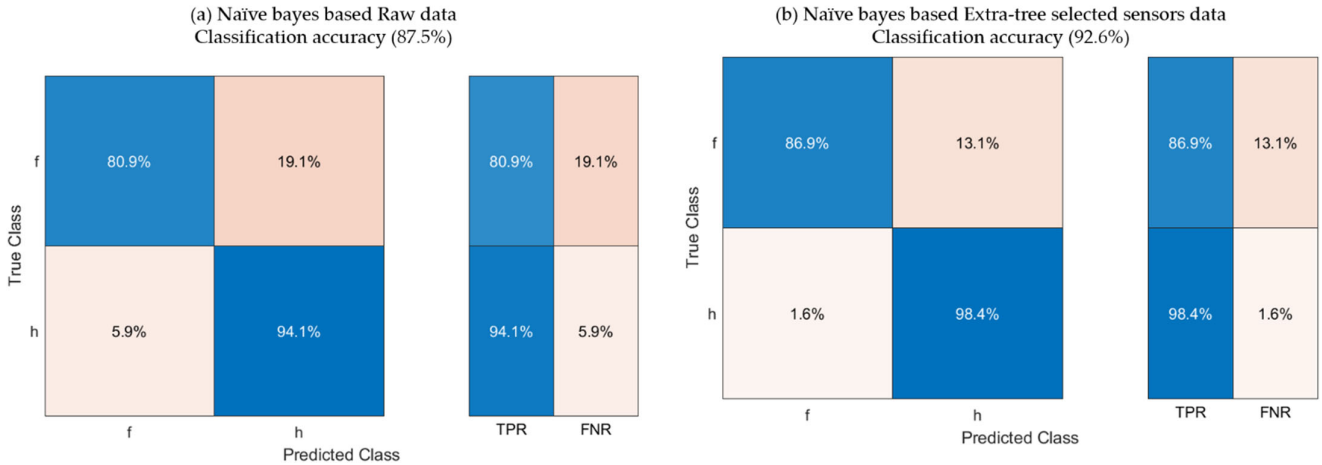

Figure 22. (**a**) Confusion matrix for the naïve-Bayes-based raw data case scenario; (**b**) confusion matrix for the naïve-Bayes-based extra-tree classifier case scenario.

Similarly, as performed earlier in the boiler water wall tube leakage case scenario, the robustness of the model is validated by performing tenfold cross-validation. The results of the tenfold cross-validation are compared with the fivefold cross-validation results. It was observed that there is a slight enhancement of cross-validation accuracies in tenfold cross-validation for both the raw and optimal sensor dataset cases, as shown in Table 7.

Table 7. Comparison of fivefold and tenfold cross-validation accuracies for the turbine motor fault detection scenario.

	Fivefold Cross-Validation Accuracies (%)			Tenfold Cross Validation Accuracies (%)		
	SVM	**k-NN**	**Naïve Bayes**	**SVM**	**k-NN**	**Naïve Bayes**
Raw data	81.2	82.4	87.5	83.8	83.5	88.6
Correlation analysis	81.1	82.7	88.6	82.0	83.1	90.2
mRMR algorithm	84.4	83.6	90.3	84.9	83.9	91.5
Extra-tree classifier	87.7	86.0	92.6	88.1	86.8	93.0

5. Conclusions

A vast number of sensor data was collected from the historical database of power plants. It is essential to point out the informative sensors necessary to detect the fault in the presence of irrelevant and redundant sensors. Multivariate algorithms are highly dependent on the number of input sensors. The redundant and irrelevant sensors may reduce the performance of these classifiers. Therefore, this study proposed a machine-learning-based optimal sensor selection approach for equipment (boiler and turbine) fault detection in thermal power plants. Three optimal sensor selection approaches (correlation analysis, mRMR algorithm, and extra-tree classifier) are employed in this study. Three supervised machine-learning classifiers (SVM, k-NN, and naïve Bayes) are used to classify the normal and faulty states. The proposed approach is implemented on the two real-world case scenarios (boiler water wall tube leakage and turbine motor fault). The computational results indicate that the optimal sensor selection approaches not only reduced the number of sensors by up to 44% in the water wall tube leakage scenario from 38 to 21 sensors, and by 55% in the turbine fault case scenario from 136 to 61 sensors, but also enhanced the machine-learning accuracy. The k-NN-based mRMR algorithm provides the highest accuracy of up to 97.6% in the boiler water wall tube leakage case scenario. In the second case scenario (turbine motor failure), the naïve-Bayes-based extra-tree classifier provides the highest accuracy of 92.6% compared with the other comparative models. This study suggests the efficient and straightforward optimal sensor selection approaches that can be implemented in thermal power plants, and in future research work, this may provide the guidelines for efficient fault detection in TPPs.

Author Contributions: Conceptualization, H.S.K. and S.K.; methodology, S.K., and H.H.; software, S.K. and H.H.; formal analysis, S.K.; resources, H.S.K.; writing—original draft preparation, S.K.; writing—review and editing, S.K. and H.S.K.; supervision, H.S.K. All authors have read and agreed to the published version of the manuscript.

Funding: This research was funded by the research project (R17GA08) of the Korea Electric Power Corporation and BK-21 four.

Institutional Review Board Statement: Not applicable.

Informed Consent Statement: Not applicable.

Data Availability Statement: Not applicable.

Acknowledgments: This research was conducted as part of the research project (R17GA08) of the Korea Electric Power Corporation and BK-21 four.

Conflicts of Interest: The authors declare that they have no conflict of interest.

List of Abbreviations

TPP	thermal power plant
PCA	principal component analysis
SVM	support vector machine
k-NN	k-nearest neighbors
NB	naïve Bayes
LDA	linear discriminant analysis

SH I	Superheater I
SH II	Superheater II
SH III	Superheater III
RH I	Reheater I
RH II	Reheater II
mRMR	maximum relevance minimum redundancy
P&ID	piping and instrumentation diagram
ANFIS	adaptive neuro-fuzzy inference
ANN	artificial neural network

Appendix A

ID	Description	Notation	ID	Description	Notation
P1CHA01GH001XQ01	Gen. Active Power	X1	P1HAH72CT003XQ01	Steam Temperature After SH II	X20
P1HAH55CT001XQ01	SH I Inlet Header Temperature	X2	P1HAH77CT001XQ01	SH III Metal Temperature	X21
P1HAH55CT002XQ01	SH I Inlet Header Temperature	X3	P1HAH77CT002XQ01	SH III Metal Temperature	X22
P1HAH55CT003XQ01	SH I Inlet Header Temperature	X4	P1HAH77CT003XQ01	SH III Metal Temperature	X23
P1HAH62CT001XQ01	Steam Temperature After SH I	X5	P1HAH77CT004XQ01	SH III Metal Temperature	X24
P1HAH62CT002XQ01	Steam Temperature After SHI	X6	P1HAH77CT005XQ01	SH III Metal Temperature	X25
P1HAH57CT001XQ01	SH I Metal Temperature	X7	P1HAJ15CT001XQ01	RH I Metal Temperature	X26
P1HAH57CT002XQ01	SH I Metal Temperature	X8	P1HAJ15CT002XQ01	RH I Metal Temperature	X27
P1HAH57CT003XQ01	SH I Metal Temperature	X9	P1HAJ15C003XQ01	RH I Metal Temperature	X28
P1HAH57CT004XQ01	SH I Metal Temperature	X10	P1HAJ15CT004XQ01	RH I Metal Temperature	X29
P1HAH57CT005XQ01	SH I Metal Temperature	X11	P1HAJ15CT005XQ01	RH I Metal Temperature	X30
P1HAH57CT006XQ01	SH I Metal Temperature	X12	P1HAJ15CT006XQ01	RH I Metal Temperature	X31
P1HAH67CT001XQ01	SH II Metal Temperature	X13	P1HAJ20CT001XQ01	RH I Outlet Steam Temperature	X32
P1HAH67CT002XQ01	SH II Metal Temperature	X14	P1HAJ35CT001XQ01	RH II Metal Temperature	X33
P1HAH67CT003XQ01	SH II Metal Temperature	X15	P1HAJ35CT002XQ01	RH II Metal Temperature	X34
P1HAH67CT004XQ01	SH II Metal Temperature	X16	P1HAJ35CT003XQ01	RH II Metal Temperature	X35
P1HAH67CT005XQ01	SH II Metal Temperature	X17	P1HAJ35CT004XQ01	RH II Metal Temperature	X36
P1HAH72CT001XQ01	Steam Temperature After SH II	X18	P1HAJ35CT005XQ01	RH II Metal Temperature	X37
P1HAH72CT002XQ01	Steam Temperature After SH II	X19	P1HAJ35CT006XQ01	RH II Metal Temperature	X38

Figure A1. Summary of the sensitive sensor data from thermal power plant boiler water wall tube leakage detection.

ID	Description	Notation	ID	Description	Notation
7DH-MW.XQ21	MW ACTUAL LOAD	X1	7S1TT-G2M1.XQ31	TBN/GEN BRG #2 MTL TMP	X69
7TB-PT01A.XQ01	P TBN 1st STG	X2	7S1TT-G3M1.XQ31	TBN/GEN BRG #3 MTL TMP	X70
7TB-PT01B.XQ01	P TBN 1st STG	X3	7S1TT-G4M1.XQ31	TBN/GEN BRG #4 MTL TMP	X71
7TB-PT01C.XQ01	P TBN 1st STG	X4	7S1TT-G5M1.XQ31	TBN/GEN BRG #5 MTL TMP	X72
S7.FSP	First Stage Shell Pressure	X5	7S1TT-G6M1.XQ31	TBN/GEN BRG #6 MTL TMP	X73
7DH-SPDO.XQ21	SPEED MAIN TBN	X6	7S1TT-G7M1.XQ31	TBN/GEN BRG #7 MTL TMP	X74
7S1TNH-RPM.XQ31	HP TBN SPD (RPM)	X7	7S1TT-G8M1.XQ31	TBN/GEN BRG #8 MTL TMP	X75
7CR-PT02A.XQ01	P CRH LN-A STM	X8	7S1TT-G9M1.XQ31	TBN/GEN BRG #9 MTL TMP	X76
7CR-PT02B.XQ01	P CRH LN-B STM	X9	7S1TT-TAM1.XQ31	TBN Thrust Active Upper MTL Temp	X77
7CR-PT03A.XQ01	P HP TBN EXH-1	X10	7S1TT-TAM2.XQ31	TBN Thrust Active Lower MTL Temp	X78
7CR-PT03B.XQ01	P HP TBN EXH-2	X11	7S1TT-TIM1.XQ31	TBN Thrust Inactive UPP MTL Temp	X79
S7.TP_HPE_P	HP Exhaust Pressure	X12	7S1TT-TIM2.XQ31	TBN Thrust Inactive LWL MTL Temp	X80
S7.TT_ES	HP Exhaust Steam Temperature	X13	S7.TT_TAD	Active Thrust Bearing Oil Drain Temperature	X81
S7.TT_ES1	HP Exhaust Steam Temperature #1	X14	S7.TT_TID	Inactive Thrust Bearing Oil Drain Temperature	X82
S7.TT_ES2	HP Exhaust Steam Temperature #2	X15	S7.TT_G1M1	Turbine/Generator Bearing #1 Metal Temperature #1	X83
S7.TT_ES3	HP Exhaust Steam Temperature #3	X16	S7.TT_G2M1	Turbine/Generator Bearing #2 Metal Temperature #1	X84
S7.TT_HPEXHLI1	HP Exhaust Lower Inner Metal Temperature #1	X17	S7.TT_G3M1	Turbine/Generator Bearing #3 Metal Temperature #1	X85
S7.TT_HPEXHLI2	HP Exhaust Lower Inner Metal Temperature #2	X18	S7.TT_G4M1	Turbine/Generator Bearing #4 Metal Temperature #1	X86
S7.TT_HPEXHUI1	HP Exhaust Upper Inner Metal Temperature #1	X19	S7.TT_G5M1	Turbine/Generator Bearing #5 Metal Temperature #1	X87
7CR-TT01A.XQ01	T CRH LN-A STM	X20	S7.TT_G6M1	Turbine/Generator Bearing #6 Metal Temperature #1	X88
7CR-TT02A.XQ01	T CRH LN-A STM	X21	S7.TT_G7M1	Turbine/Generator Bearing #7 Metal Temperature #1	X89
7CR-TT03A.XQ01	T CRH LN-A STM	X22	S7.TT_G8M1	Turbine/Generator Bearing #8 Metal Temperature #1	X90
7CR-TT01B.XQ01	T CRH LN-B STM	X23	S7.TT_G9M1	Turbine/Generator Bearing #9 Metal Temperature #1	X91
7CR-TT02B.XQ01	T CRH LN-B STM	X24	S7.TT_LPA1	Exhaust Hood A Gen end temperature #1	X92
7CR-TT03B.XQ01	T CRH LN-B STM	X25	S7.TT_LPA2	Exhaust Hood A Gen end temperature #2	X93
7HR-PT01A.XQ01	P HRH LN-A STM	X26	S7.TT_LPA3	Exhaust Hood A Gen end temperature #3	X94
7HR-PT01B.XQ01	P HRH LN-B STM	X27	S7.TT_LPB1	Exhaust Hood B Gen end temperature #1	X95
S7.HRHP_P	Hot Reheat Pressure in PSI	X28	S7.TT_LPB2	Exhaust Hood B Gen end temperature #2	X96
7HR-PT51A.XQ01	P HRH OUTL_A	X29	S7.TT_LPB3	Exhaust Hood B Gen end temperature #3	X97
7HR-PT51B.XQ01	P HRH OUTL_B	X30	S7.TT_GSEXH	Gland Seal Exhaust Temperature	X98
BFPT7A.A_AXIAL1	Axial Position #1	X31	S7.TT_SSH	Steam Seal Header Temperature	X99
BFPT7A.A_AXIAL2	Axial Position #2	X32	S7.T2_HP	HP Turbine Rotor Bore Temperature	X100
BFPT7A.A_AXIAL3	Axial Position #3	X33	S7.T2_RH	Reheat Turbine Rotor Bore Temperature	X101
7S1BB1X.XQ31	VIB 1X - BRG #1	X34	S7.T2_XO	Reheat Exhaust Rotor Bore Temperature	X102
7S1BB1Y.XQ31	VIB 1Y - BRG #1	X35	7HE-FT02A.XQ01	F IP EXT TO BFPT-A STM	X103
7S1BB2X.XQ31	VIB 2X - BRG #2	X36	7HE-FT02B.XQ01	F IP EXT TO BFPT-B STM	X104
7S1BB2Y.XQ31	VIB 2Y - BRG #2	X37	7HE-PT03A.XQ01	P IP EXT TO BFPT-A STM	X105
7S1BB3X.XQ31	VIB 3X - BRG #3	X38	7HE-PT03B.XQ01	P IP EXT TO BFPT-B STM	X106
7S1BB3Y.XQ31	VIB 3Y - BRG #3	X39	7HE-TT02A.XQ01	T IP EXT TO BFPT-A STM	X107
7S1BB4X.XQ31	VIB 4X - BRG #4	X40	7HE-TT01.XQ01	T IP EXT TO DEA STM	X108
7S1BB4Y.XQ31	VIB 4Y - BRG #4	X41	S7.EV_PA1	Exhaust Vacuum #1 LPA Hood	X109
7S1BB5X.XQ31	VIB 5X - BRG #5	X42	S7.EV_PA2	Exhaust Vacuum #2 LPA Hood	X110
7S1BB5Y.XQ31	VIB 5Y - BRG #5	X43	S7.EV_PA3	Exhaust Vacuum #3 LPA Hood	X111
7S1BB6X.XQ31	VIB 7X - BRG #6	X44	S7.EV_PB1	Exhaust Vacuum #1 LPB Hood	X112
7S1BB6Y.XQ31	VIB 6Y - BRG #6	X45	S7.EV_PB2	Exhaust Vacuum #2 LPB Hood	X113
7S1BB7X.XQ31	VIB 7X - BRG #7	X46	S7.EV_PB3	Exhaust Vacuum #3 LPB Hood	X114
7S1BB7Y.XQ31	VIB 7Y - BRG #7	X47	S7.HYD	Hydraulic Fluid Pressure	X115
7S1BB8X.XQ31	VIB 8X - BRG #8	X48	S7.HYD_PUR1	H2 Analyzer #1 Purity	X116
7S1BB8Y.XQ31	VIB 8Y - BRG #8	X49	7S7-L71EQAT	HFP TANK OIL LEVEL Tx	X117
7S1BB9X.XQ31	VIB 9X - BRG #9	X50	S7.SQP	Seal Oil Differential Pressure	X118
7S1BB9Y.XQ31	VIB 9Y - BRG #9	X51	S7.TT_G1D	Bearing #1 Oil Drain Temperature	X119
7S1BHDR.XQ31	BRG HDR PRES	X52	S7.TT_G2D	Bearing #2 Oil Drain Temperature	X120
S7.BHDR	Bearing Header Pressure	X53	S7.TT_G3D	Bearing #3 Oil Drain Temperature	X121
7S1DIFF1-EXP.XQ31	DIFF EXPNSN #1	X54	S7.TT_G4D	Bearing #4 Oil Drain Temperature	X122
7S1ROTOR-EXP1.XQ31	ROTR EXPNSN #1	X55	S7.TT_G5D	Bearing #5 Oil Drain Temperature	X123
S7.ROTOR_EXP1	Rotor Expansion #1	X56	S7.TT_G6D	Bearing #6 Oil Drain Temperature	X124
7S1SED1.XQ31	SHELL EXPNSN	X57	S7.TT_G7D	Bearing #7 Oil Drain Temperature	X125
S7.DIFF1_EXP	Differential Expansion #1	X58	S7.TT_G8D	Bearing #8 Oil Drain Temperature	X126
S7.DIFF1B_EXP	Differential Expansion #1B	X59	S7.TT_G9D	Bearing #9 Oil Drain Temperature	X127
7S1ECCENT.XQ31	ECCENTRICITY	X60	7S1XOP.XQ31	Cross Over Pipe Press	X128
7S1FSP.XQ31	1STG SHELL PRES	X61	7S1TT-XOU-CS.XQ31	C_OVER MTL TMP	X129
7CC-TT05.XQ01	T MAIN TBN LO CLR OUTL	X62	7S1TT-XOU1.XQ31	CROSS OVER PIPE TEMP1	X130
7LO-TT32.XQ01	T MAIN TBN L/O FM CLR	X63	7S1TT-XOU2.XQ31	CROSS OVER PIPE TEMP2	X131
7S7-L71QAT	Lube Oil Tank Level Transmitter	X64	7HR-PT05A.XQ01	P UPSTR LP BP_A	X132
S7.TT_LOCIA	LUBE OIL COOLER INLET TEMP	X65	7HR-PT05B.XQ01	P UPSTR LP BP_B	X133
S7.TT_LOCO	Lube Oil Cooler Outlet Temperature	X66	7HR-PT05C.XQ01	P UPSTR LP BP_C	X134
7MS-FT01-FCN.XQ03	F MAIN STEAM	X67	7HR-PT06A.XQ01	P DWNSTR LP BP RIGHT	X135
7S1TT-G1M1.XQ31	TBN/GEN BRG #1 MTL TMP	X68	7HR-PT06B.XQ01	P DWNSTR LP BP LEFT	X136

Figure A2. Summary of the sensitive sensor data from thermal power plant boiler turbine motor fault detection.

References

1. Basu, S.; Debnath, A.K. *Power Plant Instrumentation and Control Handbook: A Guide to Thermal Power Plants*; Academic Press: Cambridge, MA, USA, 2015; ISBN 978-0-12-800940-6.
2. Zhang, S.; Shen, G.; An, L. Leakage location on water-cooling wall in power plant boiler based on acoustic array and a spherical interpolation algorithm. *Appl. Therm. Eng.* **2019**, *152*, 551–558, https://doi.org/10.1016/j.applthermaleng.2019.02.073.

3. An, L.; Wang, P.; Sarti, A.; Antonacci, F.; Shi, J. Hyperbolic boiler tube leak location based on quaternary acoustic array. *Appl. Therm. Eng.* **2011**, *31*, 3428–3436, https://doi.org/10.1016/j.applthermaleng.2011.06.028.
4. Khalid, S.; Lim, W.; Kim, H.S.; Oh, Y.T.; Youn, B.D.; Kim, H.-S.; Bae, Y.-C. Intelligent Steam Power Plant Boiler Waterwall Tube Leakage Detection via Machine Learning-Based Optimal Sensor Selection. *Sensors* **2020**, *20*, 6356, https://doi.org/10.3390/s20216356.
5. Singh, P.M.; Mahmood, J. Stress Assisted Corrosion of Waterwall Tubes in Recovery Boiler Tubes: Failure Analysis. *J. Fail. Anal. Prev.* **2007**, *7*, 361–370, https://doi.org/10.1007/s11668-007-9063-z.
6. Liu, S.; Wang, W.; Liu, C. Failure analysis of the boiler water-wall tube. *Case Stud. Eng. Fail. Anal.* **2017**, *9*, 35–39, https://doi.org/10.1016/j.csefa.2017.06.002.
7. Yang, P.; Liu, S.S. Fault Diagnosis for Boilers in Thermal Power Plant by Data Mining. In Proceedings of the ICARCV 2004 8th Control, Automation, Robotics and Vision Conference, Kunming, China, 6–9 December 2004; Volume 3, pp. 2176–2180.
8. Fortuna, L.; Graziani, S.; Rizzo, A.; Xibilia, M.G. *Soft Sensors for Monitoring and Control of Industrial Processes; Advances in Industrial Control*; Springer: London, UK, 2007; ISBN 978-1-84628-479-3.
9. Yu, J.; Yoo, J.; Jang, J.; Park, J.H.; Kim, S. A novel plugged tube detection and identification approach for final super heater in thermal power plant using principal component analysis. *Energy* **2017**, *126*, 404–418, https://doi.org/10.1016/j.energy.2017.02.154.
10. Indrawan, N.; Shadle, L.J.; Breault, R.W.; Panday, R.; Chitnis, U.K. Data analytics for leak detection in a subcritical boiler. *Energy* **2020**, *220*, 119667, https://doi.org/10.1016/j.energy.2020.119667.
11. Swiercz, M.; Mroczkowska, H. Multiway PCA for Early Leak Detection in a Pipeline System of a Steam Boiler—Selected Case Studies. *Sensors* **2020**, *20*, 1561, https://doi.org/10.3390/s20061561.
12. Bhatt, M.S.; Rajkumar, N. Performance Enhancement in Coal Fired Thermal Power Plants. Part II: Steam Turbines. *Int. J. Energy Res.* **1999**, 27, 489–515.
13. Dhini, A.; Kusumoputro, B.; Surjandari, I. Neural Network Based System for Detecting and Diagnosing Faults in Steam Turbine of Thermal Power Plant. In Proceedings of the 2017 IEEE 8th International Conference on Awareness Science and Technology (iCAST), Taichung, China, 8–10 November 2017; pp. 149–154.
14. Salahshoor, K.; Khoshro, M.S.; Kordestani, M. Fault detection and diagnosis of an industrial steam turbine using a distributed configuration of adaptive neuro-fuzzy inference systems. *Simul. Model. Pr. Theory* **2011**, *19*, 1280–1293, https://doi.org/10.1016/j.simpat.2011.01.005.
15. Zhang, X.; Chen, S.; Zhu, Y.; Yan, W. Fault Detection and Diagnosis for Steam Turbine Based on Kernel GDA. In Proceedings of the 2011 International Conference on Modelling, Identification and Control, Shanghai, China, 26–29 June 2011; pp. 58–62.
16. Lin, T.-H.; Wu, S.-C. Sensor fault detection, isolation and reconstruction in nuclear power plants. *Ann. Nucl. Energy* **2018**, *126*, 398–409, https://doi.org/10.1016/j.anucene.2018.11.044.
17. han Kim, K.; seok Lee, H.; hwan Kim, J.; Park, J.H. Detection of Boiler Tube Leakage Fault in a Thermal Power Plant Using Machine Learning Based Data Mining Technique. In Proceedings of the 2019 IEEE International Conference on Industrial Technology (ICIT), Melbourne, Australia, 13–15 February 2019; pp. 1006–1010.
18. Jing, C.; Hou, J. SVM and PCA based fault classification approaches for complicated industrial process. *Neurocomputing* **2015**, *167*, 636–642, https://doi.org/10.1016/j.neucom.2015.03.082.
19. Li, W.; Peng, M.; Wang, Q. Fault identification in PCA method during sensor condition monitoring in a nuclear power plant. *Ann. Nucl. Energy* **2018**, *121*, 135–145, https://doi.org/10.1016/j.anucene.2018.07.027.
20. Young-Hun kim, J.K. Leakage Detection of a Boiler Tube Using a Genetic Algorithm-like Method and Support Vector Machines. In Proceedings of the Tenth International Conference on Soft Computing and Pattern Recognition (SoCPaR 2018), Porto, Portugal, 13–15 December 2018, doi:10.1007/978-3-030-17065-3_9.
21. Tariq, R.; Hussain, Y.; Sheikh, N.; Afaq, K.; Ali, H.M. Regression-Based Empirical Modeling of Thermal Conductivity of CuO-Water Nanofluid using Data-Driven Techniques. *Int. J. Thermophys.* **2020**, *41*, 1–28, https://doi.org/10.1007/s10765-020-2619-9.
22. Sugumaran, V.; Muralidharan, V.; Ramachandran, K. Feature selection using Decision Tree and classification through Proximal Support Vector Machine for fault diagnostics of roller bearing. *Mech. Syst. Signal Process.* **2007**, *21*, 930–942, https://doi.org/10.1016/j.ymssp.2006.05.004.
23. Chen, K.-Y.; Chen, L.-S.; Chen, M.-C.; Lee, C.-L. Using SVM based method for equipment fault detection in a thermal power plant. *Comput. Ind.* **2011**, *62*, 42–50, https://doi.org/10.1016/j.compind.2010.05.013.
24. Radovic, M.D.; Ghalwash, M.F.; Filipovic, N.; Obradovic, Z. Minimum redundancy maximum relevance feature selection approach for temporal gene expression data. *BMC Bioinform.* **2017**, *18*, 1–14, https://doi.org/10.1186/s12859-016-1423-9.
25. Sharaff, A.; Gupta, H. Extra-Tree Classifier with Metaheuristics Approach for Email Classification. In *Advances in Computer Communication and Computational Sciences*; Bhatia, S.K., Tiwari, S., Mishra, K.K., Trivedi, M.C., Eds.; Advances in Intelligent Systems and Computing; Springer Singapore: Singapore, 2019; Volume 924, pp. 189–197, ISBN 9789811368608.
26. Sun, X.; Chen, A.T.; Marquez, H.J. Boiler Leak Detection Using a System Identification Technique. *Ind. Eng. Chem. Res.* **2002**, *41*, 5447–5454, https://doi.org/10.1021/ie010949+.
27. Afgan, N.; Coelho, P.; Carvalho, M.D.G. Boiler tube leakage detection expert system. *Appl. Therm. Eng.* **1998**, *18*, 317–326, https://doi.org/10.1016/s1359-4311(97)00054-9.
28. Sun, X.; Marquez, H.J.; Chen, T.; Riaz, M. An improved PCA method with application to boiler leak detection. *ISA Trans.* **2005**, *44*, 379–397, https://doi.org/10.1016/s0019-0578(07)60211-0.

29. Lang, F.D.; Rodgers, D.A.T.; Mayer, L.E. DETECTION OF TUBE LEAKS AND THEIR LOCATION USING INPUT/LOSS METHODS. In Proceedigns of the ASME Power Conference, Baltimore, MD, USA, 30 March–1 April 2004; Volume 41626, pp. 143–150.
30. Nozari, H.A.; Shoorehdeli, M.A.; Simani, S.; Banadaki, H.D. Model-based robust fault detection and isolation of an industrial gas turbine prototype using soft computing techniques. *Neurocomputing* **2012**, *91*, 29–47, https://doi.org/10.1016/j.neucom.2012.02.014.
31. Liu, Y.; Su, M. Nonlinear Model Based Diagnostic of Gas Turbine Faults: A Case Study. In Proceedings of the Volume 3: Controls, Diagnostics and Instrumentation; Education; Electric Power; Microturbines and Small Turbomachinery; Solar Brayton and Rankine Cycle (ASMEDC), Vancouver, BC, Canada, 1 January 2011; pp. 1–8.
32. Ismail, F.B.; Singh, D.; Maisurah, N.; Musa, A.B.B. Early tube leak detection system for steam boiler at KEV power plant. *MATEC Web Conf.* **2016**, *74*, 6, https://doi.org/10.1051/matecconf/20167400006.
33. Bhatt, M.S.; Jothibasu, S. Performance Enhancement in Coal Fired Thermal Power Plants. Part I: Boilers. *Int. J. Energy Res.* **1999**, *23*, 1239–1266.
34. Kokkinos, A. *Coal R&D Beyond 2020. DOE-NETL-EPRI Technical Exchange Meeting*; EPRI: Pittsburgh, PA, USA, 2019.
35. Yong Sun; Lin Ma; Robinson, W.; Fidge, C. Using Decision Trees in Economizer Repair Decision Making. In Proceedings of the 2010 Prognostics and System Health Management Conference, Macao, China, 12–14 January 2010; pp. 1–6.
36. Liu, K.; Feng, X.; Ma, K.; Wang, L.; Xie, X.; Lu, Z. Investigation on the welding-induced multiple failures in boiler water wall tube. *Eng. Fail. Anal.* **2020**, *121*, 104988, https://doi.org/10.1016/j.engfailanal.2020.104988.
37. Yang, G.; Gou, Y.; Liu, X.; Zhang, X.; Zhang, T. Failure Analysis of the Corroded Water Wall Tube in a 50MW Thermal Power Plant. *High Temp. Mater. Process.* **2018**, *37*, 995–999, https://doi.org/10.1515/htmp-2017-0133.
38. Xue, S.; Guo, R.; Hu, F.; Ding, K.; Liu, L.; Zheng, L.; Yang, T. Analysis of the causes of leakages and preventive strategies of boiler water-wall tubes in a thermal power plant. *Eng. Fail. Anal.* **2020**, *110*, 104381, https://doi.org/10.1016/j.engfailanal.2020.104381.
39. Tanuma, T. Introduction to steam turbines for power plants. In *Advances in Steam Turbines for Modern Power Plants*; Elsevier: Amsterdam, The Netherlands, 2017; pp. 3–9 ISBN 978-0-08-100314-5.
40. Nagar, A.; Mehta, S. Steam Turbine Lube Oil System Protections Using SCADA & PLC. In Proceedings of the 2017 International Conference on Intelligent Computing and Control Systems (ICICCS), Madurai, India, 15–16 June 2017; pp. 1376–1381.
41. Dias, C.G.; Pereira, F.H. Broken Rotor Bars Detection in Induction Motors Running at Very Low Slip Using a Hall Effect Sensor. *IEEE Sens. J.* **2018**, *18*, 4602–4613, https://doi.org/10.1109/jsen.2018.2827204.
42. Niu, J.; Lu, S.; Liu, Y.; Zhao, J.; Wang, Q. Intelligent Bearing Fault Diagnosis Based on Tacholess Order Tracking for a Variable-Speed AC Electric Machine. *IEEE Sens. J.* **2018**, *19*, 1850–1861, https://doi.org/10.1109/jsen.2018.2883955.
43. Fu, Q.; Jing, B.; He, P.; Si, S.; Wang, Y. Fault Feature Selection and Diagnosis of Rolling Bearings Based on EEMD and Optimized Elman_AdaBoost Algorithm. *IEEE Sens. J.* **2018**, *18*, 5024–5034, https://doi.org/10.1109/jsen.2018.2830109.
44. Rao, S.G.; Lohith, S.; Gowda, P.C.; Singh, A.; Rekha, S.N. Fault Analysis of Induction Motor. In Proceedings of the 2019 IEEE International Conference on Intelligent Techniques in Control, Optimization and Signal Processing (INCOS); Tamilnadu, India, 11-13 April 2019; pp. 1–4.
45. Moradi, M.; Chaibakhsh, A.; Ramezani, A. An intelligent hybrid technique for fault detection and condition monitoring of a thermal power plant. *Appl. Math. Model.* **2018**, *60*, 34–47, https://doi.org/10.1016/j.apm.2018.03.002.
46. Shaheryar, A.; Yin, X.-C.; Hao, H.-W.; Ali, H.; Iqbal, K. A Denoising Based Autoassociative Model for Robust Sensor Monitoring in Nuclear Power Plants. *Sci. Technol. Nucl. Install.* **2016**, *2016*, 1–17, https://doi.org/10.1155/2016/9746948.
47. Yoshizawa, T.; Hirobayashi, S.; Misawa, T. Noise reduction for periodic signals using high-resolution frequency analysis. *EURASIP J. Audio Speech Music. Process.* **2011**, *2011*, 5, https://doi.org/10.1186/1687-4722-2011-426794.
48. Curling, L.; Gagnon, J.; Paidoussis, M. Noise removal from power spectral densities of multicomponent signals by the coherence method. *Mech. Syst. Signal Process.* **1992**, *6*, 17–27, https://doi.org/10.1016/0888-3270(92)90053-l.
49. Abbasi, A.R.; Rafsanjani, A.; Farshidianfar, A.; Irani, N. Rolling element bearings multi-fault classification based on the wavelet denoising and support vector machine. *Mech. Syst. Signal Process.* **2007**, *21*, 2933–2945, https://doi.org/10.1016/j.ymssp.2007.02.003.
50. Wang, Z.; Zhang, Q.; Xiong, J.; Xiao, M.; Sun, G.; He, J. Fault Diagnosis of a Rolling Bearing Using Wavelet Packet Denoising and Random Forests. *IEEE Sens. J.* **2017**, *17*, 5581–5588, https://doi.org/10.1109/jsen.2017.2726011.
51. Risqiwati, D.; Wibawa, A.D.; Pane, E.S.; Islamiyah, W.R.; Tyas, A.E.; Purnomo, M.H. Feature Selection for EEG-Based Fatigue Analysis Using Pearson Correlation. In Proceedings of the 2020 International Seminar on Intelligent Technology and Its Applications (ISITIA), Surabaya, Indonesia, 22–23 July 2020; pp. 164–169.
52. Benesty, J.; Chen, J.; Huang, Y.; Cohen, I. Pearson Correlation Coefficient. In *Noise Reduction in Speech Processing*; Springer Topics in Signal Processing; Springer Berlin/Heidelberg: Berlin/Heidelberg, Germany, 2009; Volume 2, pp. 1–4, ISBN 978-3-642-00295-3.
53. Peng, H.; Long, F.; Ding, C. Feature selection based on mutual information criteria of max-dependency, max-relevance, and min-redundancy. *IEEE Trans. Pattern Anal. Mach. Intell.* **2005**, *27*, 1226–1238, https://doi.org/10.1109/tpami.2005.159.
54. Yan, X.; Jia, M. Intelligent fault diagnosis of rotating machinery using improved multiscale dispersion entropy and mRMR feature selection. *Knowl.-Based Syst.* **2018**, *163*, 450–471, https://doi.org/10.1016/j.knosys.2018.09.004.

55. Stetco, A.; Dinmohammadi, F.; Zhao, X.; Robu, V.; Flynn, D.; Barnes, M.; Keane, J.; Nenadic, G. Machine learning methods for wind turbine condition monitoring: A review. *Renew. Energy* **2018**, *133*, 620–635, https://doi.org/10.1016/j.renene.2018.10.047.
56. Jack, L.; Nandi, A. FAULT DETECTION USING SUPPORT VECTOR MACHINES AND ARTIFICIAL NEURAL NETWORKS, AUGMENTED BY GENETIC ALGORITHMS. *Mech. Syst. Signal Process.* **2002**, *16*, 373–390, https://doi.org/10.1006/mssp.2001.1454.
57. Guenther, N.; Schonlau, M. Support Vector Machines. *Stata J. Promot. Commun. Stat. Stata* **2016**, *16*, 917–937, https://doi.org/10.1177/1536867x1601600407.
58. Yuan, J.; Wang, C.; Zhou, Z. Study on refined control and prediction model of district heating station based on support vector machine. *Energy* **2019**, *189*, 116193, https://doi.org/10.1016/j.energy.2019.116193.
59. Vernekar, K.; Kumar, H.; Gangadharan, K.V. Engine gearbox fault diagnosis using empirical mode decomposition method and Naïve Bayes algorithm. *Sadhana* **2017**, *42*, 1143–1153, https://doi.org/10.1007/s12046-017-0678-9.
60. Schmidt, J.; Marques, M.R.G.; Botti, S.; Marques, M.A.L. Recent advances and applications of machine learning in solid-state materials science. *NPJ Comput. Mater.* **2019**, *5*, https://doi.org/10.1038/s41524-019-0221-0.